

Axion Mixing in the String Axiverse

Hai-Jun Li^a and Yu-Feng Zhou^{a,b,c,d}

^a*Key Laboratory of Theoretical Physics, Institute of Theoretical Physics, Chinese Academy of Sciences, Beijing 100190, China*

^b*School of Physical Sciences, University of Chinese Academy of Sciences, Beijing 100049, China*

^c*School of Fundamental Physics and Mathematical Sciences, Hangzhou Institute for Advanced Study, UCAS, Hangzhou 310024, China*

^d*International Centre for Theoretical Physics Asia-Pacific, Beijing/Hangzhou, China*

E-mail: lihaijun@itp.ac.cn, yfzhou@itp.ac.cn

The string axiverse presents a fascinating and complex landscape for axion physics. In this work, we study axion mass mixing within the type IIB string axiverse, focusing specifically on the LARGE volume scenario (LVS) axiverse. The LVS axiverse necessitates at least two axions to ensure the presence of both a QCD axion candidate and at least one additional axion-like particle (ALP). This study presents the first systematic exploration of axion mass mixing in scenarios involving more than two axions. The maximal mixing occurs when the masses of all ALPs are smaller than the zero-temperature mass of the QCD axion, with no two ALP masses being equal, and when the decay constants of all ALPs are simultaneously either smaller or larger than the decay constant of the QCD axion. Additionally, the transfer of axion energy density ultimately takes place only between the two axions with the closest masses. These findings provide critical insights into axion dynamics not only within type IIB string axiverse models but also in broader multi-axion mixing frameworks. The potential cosmological implications of axion mass mixing are also addressed at the end. Our work contributes to the understanding of axion physics in string theory.

April 15, 2025

Contents

1	Introduction	2
2	Axions in string theory	6
2.1	Model independent axions	6
2.2	Model dependent axions	7
3	Review of the type IIB string axiverse	8
3.1	The type IIB LARGE volume scenario axiverse	8
3.2	Specific LVS axiverse models	11
4	Axion mass mixing in the type IIB string axiverse	14
4.1	The 1 + 1 mixing scenario	14
4.2	The 1 + 2 mixing scenario	18
4.3	The 1 + N mixing scenario	25
5	Cosmological implications	31
5.1	Dark matter	31
5.2	Isocurvature fluctuations	33
5.3	Dark energy	34
5.4	Domain walls	34
5.5	Gravitational waves	35
5.6	Primordial black holes	35
6	Conclusion and outlook	36
A	Divisor volumes	37
B	Axion coupling to gauge fields	38
C	Axion relic density without mass mixing	38

1 Introduction

String theory phenomenology introduces the concept of the Axiverse — a cosmological framework predicting not only the QCD axion in the low-energy effective field theory (EFT), but also a plenitude of ultra-light axion-like particles (ALPs) [1–4]. The QCD axion, a pseudoscalar field, originates from the Peccei-Quinn (PQ) mechanism [5, 6], which postulates the spontaneously breaking of a global $U(1)_{\text{PQ}}$ symmetry. Under this PQ symmetry, the axion field ϕ transforms as $\phi \rightarrow \phi + 2\pi f_a$ (where f_a represents the axion decay constant), dynamically resolving the strong CP problem in the Standard Model (SM) by stabilizing its potential at the CP-conserving minimum [7–12]. This stabilization arises from QCD non-perturbative effects, which induce the axion potential via QCD instantons and generate a parametrically small axion mass [13, 14]. Moreover, the QCD axion serves as a compelling cold dark matter candidate. Its non-thermal production in the early Universe, driven by the misalignment mechanism [15–17], links the oscillation energy density of the axion field to the observed dark matter abundance. Recent reviews further elaborate on these aspects [18–21]. For a natural initial misalignment angle $\theta_i \sim \mathcal{O}(1)$, this mechanism constrains the QCD axion decay constant to the classical window

$$10^8 - 10^9 \text{ GeV} \lesssim f_a \lesssim 10^{11} - 10^{12} \text{ GeV}. \quad (1.1)$$

The upper bound stems from avoiding the overproduction of axion dark matter, while the lower limit is derived from astrophysical probes such as neutrino burst durations in SN 1987A [22–24] and neutron star cooling rates [25–27].

On the other hand, ultra-light ALPs with logarithmically hierarchical masses, which also encompass the QCD axion, predominantly arise from higher-dimensional gauge fields [28–30]. In the framework of string theory [31, 32], these particles can be understood as lower-dimensional axions emerging through the process of integrating higher-dimensional gauge fields over specific cycles within the compactified extra dimensions. There exist model-independent axions, which remain unaffected by the detailed structure of the internal manifold. Conversely, there also exist axions, whose decay constants are significantly influenced by the internal geometry of the compactification, giving rise to what is commonly termed the model-dependent axions. These model-independent and model-dependent axions highlight the rich interplay between higher-dimensional theories and low-energy phenomenology, thus providing a promising arena for exploring new physics beyond the SM. For further insights into the role of axions in extra-dimensional scenarios, including recent advancements and discussions, see, for example, refs. [33–35].

It was shown that the potential of an axiverse can be realized within the framework of type IIB string compactifications [36–40]. Below the compactification scale, the low-energy spectrum typically contains many ALPs, which are Kaluza-Klein (KK) zero modes of antisymmetric form fields originating from bosonic type IIB strings. Specifically, their number, which is linked to the topology of the internal manifold and particularly to the harmonic forms on a Calabi-Yau (CY) manifold, is often in the hundreds. Therefore, the low-energy theory is rich in these closed string axions. While open string axions may also exist on a brane, they are more model-dependent, so the focus here is on closed string axions in the bulk.

Each axion is accompanied by a real scalar field known as the saxion, together forming a complex field that constitutes the lowest component of a chiral superfield. The saxion and axion represent the real and imaginary parts of this complex field, respectively. Saxions are moduli that affect EFT features, and it is crucial for them to avoid mediating the unobserved fifth-forces and suffering from the cosmological moduli problem (CMP) [41–43]. Then the moduli stabilization mechanism, such as the Kachru-Kalosh-Linde-Trivedi (KKLT) scenario [44], give the moduli a heavy mass, which may also induce a potential for axions that make them too heavy. In refs. [37–39], they show that a wonderful axiverse with multiple light axions can be realized in the context of the LARGE volume scenario (LVS) [45, 46].

The type IIB string axiverse features two regimes based on the vacuum expectation value (VEV) of the tree-level superpotential W_0 . When $W_0 \ll 1$, a single non-perturbative effect creates a minimum for all Kähler moduli, lifting one axion while leaving other axions massless [36]. However, the challenges faced include identifying a rigid ample divisor and avoiding chiral intersections. When W_0 is of order one, the LVS moduli stabilization mechanism results in one heavy axion from a del Pezzo divisor fixed by non-perturbative effects and multiple light axions stabilized through perturbative effects, acquiring a potential from higher-order instanton effects [45–47]. Furthermore, some light axions could be eaten up by massive U(1) gauge bosons via the Stückelberg mechanism. The LVS axiverse requires at least two axions to guarantee the presence of both a QCD axion candidate and at least one additional ALP. Specifically, ref. [37] outlines models featuring one QCD axion plus one ALP, one QCD axion plus two ALPs, and one QCD axion plus multiple ALPs. In general, the QCD axion requires an intermediate-scale decay constant and an anomaly coefficient of order unity. In the LVS axiverse, the QCD axion with a higher-scale decay constant can be diluted by the late out-of-equilibrium decay of some heavy moduli [36]. On the other hand, within this framework, we will see that both the overproduction and underproduction of dark matter abundance of the QCD axion (or ALPs) can be naturally accounted for through their mass mixing.

In the context of the axiverse, it is natural to consider the cosmological evolution of multiple axions, which has been extensively studied in recent years [48–51]. When non-zero mass mixing between two axions is considered, a non-trivial cosmological evolution of the mass eigenvalues, known as level crossing, can occur during the QCD phase transition. Examples include the mixing between the QCD axion and an ALP [49], between the QCD axion and a sterile axion [50], and between the Z_N axion [52–54] and an ALP [51], among others. Generally, level crossing can take place before the critical temperature of the QCD phase transition, T_{QCD} . However, as highlighted in ref. [51], this is not always the case, as a second level crossing might occur at T_{QCD} in scenarios involving a Z_N axion — a phenomenon referred to as double level crossings (see also ref. [55] for another example). The level crossing can induce an adiabatic transition in the axion energy density, analogous to the Mikheyev-Smirnov-Wolfenstein (MSW) effect [56–58] observed in neutrino oscillations. It also carries profound cosmological implications, such as altering the axion relic density [59–63] and isocurvature perturbations [49, 64], contributing to the composition of dark energy [65, 66], influencing the formation of domain walls [67–69], and impacting gravitational waves and primordial black holes [69–74], among other effects.

The examples mentioned above all consider mass mixing between two axions, with the selection of axions generally being relatively arbitrary. However, in this work, our focus will be on axion mass mixing within the framework of the type IIB string axiverse. Furthermore, and more importantly, for the first time, we will investigate mass mixing in scenarios where the number of axions exceeds two. Specifically, we will delve into several mixing scenarios, including the mixing of one QCD axion with one ALP (the $1 + 1$ mixing), the mixing of one QCD axion with two ALPs (the $1 + 2$ mixing), and the mixing of one QCD axion with multiple ALPs (the $1 + N$ mixing, where $N > 2$). Notice that these mixing scenarios all correspond to the theoretical framework of the type IIB LVS axiverse [37–39].

The $1 + 1$ mixing scenario is a common one that has garnered considerable attention and has been extensively studied in numerous pieces of previous literature. However, it is still necessary to clarify this scenario first within the context of the string axiverse. Predominantly, this scenario focuses on the mass mixing that occurs between the QCD axion and an ALP. More specifically, depending on the variation in the energy density of the QCD axion, it can be subdivided into two scenarios: the light QCD axion scenario [49, 51] and the heavy QCD axion scenario [50]. Additionally, it is worth noting that scenarios involving the mixing between two QCD axions have also been given considerable consideration within this framework [55, 75]. However, the $1 + 2$ and $1 + N$ mixing scenarios with more than two axions in the string axiverse have not been studied before.

In the $1 + 2$ mixing scenario, we consider both isotropic and anisotropic cases. In the isotropic case, we consider the mixing of one QCD axion and two ALPs, with both ALPs having decay constants smaller than those of the QCD axion. In the anisotropic case, we can only consider the mixing of one QCD axion and one ALP, meaning that the $1 + 2$ mixing scenario will transform into the $1 + 1$ scenario. Among them, the scenario where one ALP has a decay constant smaller than those of the QCD axion corresponds to the light QCD axion scenario, while the one with a larger decay constant corresponds to the heavy QCD axion scenario. Additionally, we will briefly discuss the isotropic case where both ALPs have decay constants larger than those of the QCD axion. Notice that in these mixing scenarios, the mass of the ALP is assumed to be constant and must be smaller than that of the QCD axion, and more precisely, the zero-temperature axion mass.

Subsequently, within the framework of the LVS axiverse, it is quite natural to extend the $1 + 2$ mixing scenario to the $1 + N$ mixing scenario. In this scenario, for effective mixing to occur, the decay constants of ALPs must be either smaller than or larger than those of the QCD axion. It is important to note that, given the assumption of constant ALP masses, the QCD axions will only mix individually with each ALP, without mass mixing occurring among the ALPs themselves. Therefore, the masses of the ALPs cannot be equal; if two ALPs have the same mass, effective mixing will only take place once. In the $1 + N$ mixing scenario, we can summarize two key conditions for the occurrence of *maximal* mixing among multiple axion mass eigenstates:

- *The masses of all ALPs must be smaller than the zero-temperature mass of the QCD axion, and no two of the ALP masses can be equal; rather, there should be a distinct mass hierarchy among them.*
- *The decay constants of all ALPs must simultaneously be either smaller than or larger than the decay constant of the QCD axion; otherwise, the maximal mixing scenario would be compromised.*

Certainly, these conclusions are based on the contemplation of the mixing scenario involving one QCD axion and multiple ALPs (all possessing constant masses) within the context of the type IIB string axiverse, but they should also be applicable to more generalized multi-axion mixing scenarios. We also find that the transfer of axion energy density ultimately only occurs between the two axions with the closest masses, and this applies equally to both the $1 + 1$ and $1 + 2$ mixing scenarios. In addition, the $1 + N$ mixing scenario where all ALPs have decay constants larger than the QCD axion is also briefly discussed.

Lastly, as mentioned earlier, axion mass mixing in the string axiverse has rich phenomenology. We will briefly discuss its cosmological implications, including axion relic density, isocurvature fluctuations, dark energy, domain walls, gravitational waves, and primordial black holes. Notice that the string axiverse also possesses rich phenomenological aspects but unrelated to axion mass mixing, see e.g. refs. [76–96].

The rest of this paper is structured as follows. In section 2, we provide a concise overview of axions in string theory. In section 3, we introduce the type IIB string axiverse. We first introduce the concept of the LVS axiverse and then present several specific LVS axiverse models. In section 4, we investigate axion mass mixing in the type IIB string axiverse, specifically, with the $1 + 1$, $1 + 2$, and $1 + N$ mixing scenarios. The cosmological implications of axion mass mixing are included in section 5. Finally, the conclusion and outlook are given in section 6.

2 Axions in string theory

In this section, we briefly review axions within the context of string theory [31], see also ref. [97] for a recent overview. There are two methods in string theory for reducing the p -form gauge field C_p to the string theory axion under the compactification: model-independent axions and model-dependent axions. The first method involves dualizing the 2-form gauge field in four non-compact spacetime dimensions, a process that is unrelated to the structure of the internal manifold. Conversely, the second method arises from C_p components that are aligned with the directions of the compact internal manifold; in the moduli space, this determination is influenced by the structure of the internal manifold.

2.1 Model independent axions

Considering the dualized Kalb-Ramond 2-form B_2 in the heterotic string theory, the relevant effective action is given by

$$-\frac{2\pi}{g_s^2 \ell_s^4} \int \frac{1}{2} H_3 \wedge \star_{10} H_3 - \frac{1}{8\pi g_s^2 \ell_s^6} \int \text{Tr}(F \wedge \star_{10} F), \quad (2.1)$$

where \wedge is the wedge product, \star is the Hodge star operation, g_s and l_s are the string coupling constant and length, respectively, and H_3 is the field strength of B_2 as

$$dH_3 = \frac{1}{16\pi^2} [\text{Tr}(R \wedge R) - \text{Tr}(F \wedge F)], \quad (2.2)$$

with the curvature 2-form R and the gauge field strength F . Notice that here $R \wedge R$ can be omitted and eq. (2.2) can be imposed on the action by introducing the 6-form

B_6 . Then integrating out H_3 in the dual field of B_2 , we can obtain

$$-\frac{g_s^2 \ell_s^4}{2\pi} \int \frac{1}{2} H_7 \wedge \star_{10} H_7 - \frac{1}{8\pi g_s^2 \ell_s^6} \int \text{Tr}(F \wedge \star_{10} F) + \frac{1}{16\pi^2} \int B_6 \wedge \text{Tr}(F \wedge F), \quad (2.3)$$

where $H_7 \equiv dB_6 = 2\pi/(g_s^2 \ell_s^4) \star_{10} H_3$, in which the heterotic string is compactified to four-dimensions on the compact internal manifold K_6 . After the KK reduction, the first and second terms in eq. (2.3) can be written as

$$-\int_{X_4} \frac{1}{2} f^2 d\theta \wedge \star_4 d\theta + \frac{1}{8\pi^2} \sum_a \int_{X_4} \frac{1}{2} \theta \text{Tr}(F^{(a)} \wedge F^{(a)}), \quad (2.4)$$

where X_4 represents the four-dimensional non-compact manifold and the axion decay constant f is given by

$$f^2 = \frac{g_s^2 \ell_s^4}{2\pi \text{Vol}(K_6)} = \frac{g_s^2}{2\pi \ell_s^2 \mathcal{V}}, \quad (2.5)$$

with the volume of the internal manifold $\text{Vol}(K_6) = \ell_s^6 \mathcal{V}$.

2.2 Model dependent axions

Furthermore, string theory encompasses various p -form gauge fields C_p where p is not confined to the value of 2. Upon being compactified on p -cycles, these fields can produce four-dimensional axions. The C_p is given by

$$C_p(x, y) = \sum_{\alpha=1}^{b_p(K_6)} \frac{\theta^\alpha(x)}{2\pi} \omega_{p,\alpha}(y), \quad (2.6)$$

where $\omega_{p,\alpha}$ ($\alpha = 1, \dots, b_p(K_6)$) represent the warped harmonic representatives. Using the inner product of two harmonic forms

$$\langle \omega_{p,\alpha}, \omega_{p,\beta} \rangle \text{Vol}(K_6) = \int_{K_6} \omega_{p,\alpha} \wedge \star_6 \omega_{p,\beta}, \quad (2.7)$$

we have the kinetic term for C_p in the string frame

$$-\frac{g_s^2}{2k_{10}^2} \int \frac{1}{2} dC_p \wedge \star dC_p = - \int_{X_4} \frac{1}{2} f_{\alpha\beta}^2 d\theta^\alpha \wedge \star_4 d\theta^\beta, \quad (2.8)$$

where k_{10} is the ten-dimensional gravitational coupling and the axion decay constant $f_{\alpha\beta}$ is given by

$$f_{\alpha\beta}^2 = \frac{g_s^2}{8\pi^2} M_{\text{Pl}}^2 \langle \omega_{p,\alpha}, \omega_{p,\beta} \rangle, \quad (2.9)$$

with the four-dimensional reduced Planck mass M_{Pl} . Upon defining the compact internal manifold K_6 by the CY three-fold, the resulting four-dimensional EFT displays $\mathcal{N} = 1$ supersymmetry in type I and heterotic string theories, whereas it exhibits $\mathcal{N} = 2$ supersymmetry in type II string theory. In these cases, both the axion and the Kähler modulus are part of the same supersymmetry multiplet and therefore can be considered as the pseudoscalar and scalar components of a complex scalar field, respectively. Notice that several axions will be removed from the low-energy spectrum.

3 Review of the type IIB string axiverse

In this section, we introduce the type IIB string axiverse [37–39]. To begin with, we will introduce the concept of the LVS axiverse, providing a foundational understanding. Subsequently, we will present several specific LVS axiverse models.

3.1 The type IIB LARGE volume scenario axiverse

In type IIB flux compactifications on CY, the SM is localized on a stack of D3 or D7 branes. The pseudo-scalar axion-like fields c^a ($a = 1, \dots, h_-^{1,1}$) and c_α ($\alpha = 1, \dots, h_+^{1,1}$) can arise as KK zero modes of the Ramond-Ramond (RR) antisymmetric tensor fields C_2 and C_4 . Here we consider the case with the Hodge number $h_-^{1,1} = 0$, i.e., all the moduli corresponding to $h_-^{1,1}$ are projected out by the orientifold involution, and thus $h^{1,1} = h_+^{1,1}$. The Kähler moduli can be described by

$$T_\alpha = \tau_\alpha + i c_\alpha, \quad (3.1)$$

where τ_α are the divisor volumes, see appendix A. To obtain the axion decay constant, we first need to perform an orthogonal transformation for the effective Lagrangian (see also appendix B), which results in the kinetic term [37]

$$\mathcal{L} \supset -\frac{1}{8} \lambda_\alpha \partial_\mu c'_\alpha \partial^\mu c'_\alpha, \quad (3.2)$$

where λ_α are the eigenvalues of $\mathcal{K}_{\alpha\beta}$. Subsequently, we need to define a new field for canonical normalization

$$a_\alpha \equiv \frac{1}{2} \sqrt{\lambda_\alpha} c'_\alpha, \quad (3.3)$$

and finally, we obtain the decay constants for canonically normalized axions

$$f_\alpha \equiv \frac{\sqrt{\lambda_\alpha} M_{\text{Pl}}}{4\pi}, \quad (3.4)$$

with the periodicity $a_\alpha = a_\alpha + 2\pi f_\alpha$. Considering the simplest Swiss-cheese CY manifold, we have the volume [98]

$$\mathcal{V} = \frac{1}{9\sqrt{2}} \left(\tau_b^{3/2} - \tau_s^{3/2} \right), \quad (3.5)$$

where τ_b and τ_s are the large and small divisor volumes, respectively. In the limit $\tau_b \gg \tau_s$, the decay constants of the corresponding axions are given by [37]

$$f_{a_b} = \frac{\sqrt{3}M_{\text{Pl}}}{4\pi\tau_b} \simeq \frac{M_{\text{Pl}}}{4\pi\mathcal{V}^{2/3}}, \quad f_{a_s} = \frac{1}{\sqrt{6}(2\tau_s)^{1/4}} \frac{M_{\text{Pl}}}{4\pi\sqrt{\mathcal{V}}} \simeq \frac{M_s}{\sqrt{4\pi\tau_s}^{1/4}}, \quad (3.6)$$

where M_s is the string scale. Now, considering fibred CY manifolds with a del Pezzo divisor, we have the volume [99]

$$\mathcal{V} = t_b t_f^2 + t_s^3, \quad (3.7)$$

where $\tau_b = 2t_b t_f$, $\tau_f = t_f^2$, and $\tau_s = 3t_s^2$ are the divisor volumes, respectively. In the limit $t_s \tau_f \gg \tau_s^{3/2}$, the decay constants of the corresponding axions are given by [37]

$$f_{a_f} = \frac{M_{\text{Pl}}}{4\pi\tau_f}, \quad f_{a_b} = \frac{\sqrt{2}M_{\text{Pl}}}{4\pi\tau_b}, \quad f_{a_s} = \frac{1}{\sqrt{2}(3\tau_s)^{1/4}} \frac{M_{\text{Pl}}}{4\pi\sqrt{\mathcal{V}}} \simeq \frac{M_s}{\sqrt{4\pi\tau_s}^{1/4}}. \quad (3.8)$$

Furthermore, there are two scenarios in which the CY can have either an isotropic or anisotropic shape. In the isotropic limit $t_b \sim \sqrt{\tau_f} \sim \mathcal{V}^{1/3}$, we have

$$f_{a_f} \simeq f_{a_b} \simeq \frac{M_{\text{Pl}}}{4\pi\mathcal{V}^{2/3}}, \quad f_{a_s} \simeq \frac{M_s}{\sqrt{4\pi\tau_s}^{1/4}}. \quad (3.9)$$

While in the anisotropic limit $t_b \sim \mathcal{V} \gg \sqrt{\tau_f} \sim \sqrt{\tau_s}$, we have

$$f_{a_f} \simeq \frac{M_{\text{Pl}}}{4\pi\tau_s}, \quad f_{a_b} \simeq \frac{M_{\text{Pl}}}{4\pi\tau_b}, \quad f_{a_s} \simeq \frac{M_s}{\sqrt{4\pi\tau_s}^{1/4}}. \quad (3.10)$$

Here we present only the axion decay constants. Another crucial factor is the coupling strength between axion and gauge bosons, especially considering the topology of the CY three-fold and the choice of brane set-up and fluxes, which determines whether it can behave as the QCD axion with an anomaly coefficient of order unity.

The type IIB string axiverse exhibits two distinct regimes, depending on the VEV of the tree-level superpotential W_0 . In the ample divisor case where $W_0 \ll 1$, the single non-perturbative effect is capable of generating a minimum for all the Kähler moduli, lifting only one axion while leaving $h^{1,1} - 1$ axions massless at leading order [36]. The

main challenges in realizing this scenario microscopically lie in finding a rigid ample divisor and avoiding chiral intersections via gauge flux selection.

On the other hand, in the case where W_0 is of order one, the LVS leads to an axiverse with one heavy axion and multiple light axions [45–47]. The heavy axion arises from a del Pezzo divisor T_{dP} fixed by the non-perturbative effects, while the light axions are stabilized perturbatively by the α' and g_s effects, and acquire a potential from higher-order instanton effects. Notice that some light axions could be eaten up by massive U(1) gauge bosons via the Stückelberg mechanism. In this context, the scalar potential comprises various contributions that scale differently with the exponentially large total volume [37, 38]

$$V = V_D + V_F^{\text{tree}} + V_F^{\text{np}} + V_F^{\text{p}}, \quad (3.11)$$

where V_D represents the D-term potential that scales as $V_D \sim \mathcal{O}(\mathcal{V}^{-2})$, V_F^{tree} represents the tree-level F-term scalar potential that scales as $V_F^{\text{tree}} \sim \mathcal{O}(\mathcal{V}^{-2})$, V_F^{np} represents the non-perturbative scalar potential that scales as $V_F^{\text{np}} \sim \mathcal{O}(\mathcal{V}^{-3})$, and V_F^{p} represents the perturbative potential from the α' and g_s corrections to the Kähler potential. The D-term conditions stabilize d combinations of Kähler moduli, resulting in $n_{\text{ax}} = h^{1,1} - d - 1$ flat directions. Consequently, the d combinations of axions are eaten up, leaving only n_{ax} axions remain light. Furthermore, it demands a minimum of $n_{\text{ax}} \geq 2$ to ensure the existence of a QCD axion candidate along with at least one additional ALP. The non-perturbative scalar potential V_F^{np} arises from corrections to the superpotential W , which stabilize T_{dP} at a small size and render the corresponding axions massive $m_{a_{\text{dP}}} \sim m_{\tau_{\text{dP}}}$ [100]. The perturbative potential V_F^{p} eliminates the remaining flat directions from the D-terms and non-perturbative effects, resulting in all corresponding axions being massless. The α' correction leads to a scalar potential that scales as $V_F^{\alpha'} \sim \mathcal{O}(\mathcal{V}^{-3})$ [101], which yields an exponentially large internal volume [45]

$$\mathcal{V} \sim W_0 e^{a\tau_{\text{dP}}}, \quad (3.12)$$

with a light volume mode mass $m_{\mathcal{V}} \sim W_0 M_{\text{Pl}} / \mathcal{V}^{3/2} \sim \sqrt{m_{3/2}^3 / M_{\text{Pl}}}$, where $a = 2\pi/n$ and $m_{3/2}$ is the gravitino mass. While the g_s correction is sub-leading and leads to a scalar potential that scales as $V_F^{g_s} \sim \mathcal{O}(\mathcal{V}^{-(3+p)})$ with $p > 0$ [102]. Then the sub-leading higher-order non-perturbative effects slightly lift the n_{ax} axion directions, resulting in the emergence of the LVS axiverse [37]

$$V_{W_{\text{np}}}(c_i) \simeq - \sum_{i=1}^{n_{\text{ax}}} \frac{n_i a_i \tau_i W_0}{\mathcal{V}^2} e^{-n_i a_i \tau_i} \cos(n_i a_i c_i). \quad (3.13)$$

In addition, axions can acquire mass through the non-perturbative corrections to the Kähler potential, which can only dominate the QCD axion potential with a single

instanton superpotential contribution [32]. In this case, the ALP masses are anticipated to be smaller than those of the QCD axion.

3.2 Specific LVS axiverse models

In this subsection, we present an array of specific type IIB LVS axiverse models sourced from refs. [37–39]. These models hold paramount significance as they will serve as the cornerstone for our investigation into axion mass mixing in the subsequent sections. Consequently, it is indispensable to gain a thorough understanding of them. Here, we show three distinct types of models: firstly, a model containing one QCD axion plus one ALP; secondly, a model featuring one QCD axion plus two ALPs; and lastly, models that encompass one QCD axion plus multiple ALPs.

3.2.1 One QCD axion plus one ALP

We first introduce a model containing one QCD axion plus one ALP from refs. [37, 38]. This is an anisotropic $SU(3) \times SU(2)$ model with $d = 1$ D-term equation leading to $n_{\text{ax}} = 2$ light axions: a fibre axion as the QCD axion, and a base axion as the light ALP. Notice that there is also another isotropic model, but it has only one QCD axion.

The internal space of this type IIB model is an orientifold of a K3 fibred CY three-fold, characterized by specific Hodge numbers $h^{1,1} = h_+^{1,1} = 4$, realized as a hypersurface in a toric variety. The key divisors for modeling include the K3 fiber D_1 , two intersecting rigid four-cycles D_4 and D_5 , and a del Pezzo divisor D_7 . The Kähler form is given by [38]

$$J = t_1 \hat{D}_1 + t_4 \hat{D}_4 + t_5 \hat{D}_5 + t_7 \hat{D}_7, \quad (3.14)$$

and the overall volume is

$$\mathcal{V} = \frac{1}{2} t_{\text{base}} \tau_1 + t_4 t_5^2 - \frac{1}{3} t_5^3 - \frac{1}{3} \tau_7^{3/2}, \quad (3.15)$$

where $t_{\text{base}} = 2(t_1 - t_5)$. The $SU(3) \times SU(2)$ model is accomplished by wrapping 3 D7-branes around D_4 and 1 D7-brane around the K3 fiber D_1 . The anomalous $U(1)$ acquires mass through the Stückelberg mechanism by eaten up a closed string axion. The gauge flux generates a moduli-dependent Fayet-Iliopoulos (FI) term, resulting in the fixation of one Kähler modulus at $\tau_4 = 3(\tau_1 - \tau_5) - \tau_7$. The three remaining Kähler moduli are τ_1 , τ_5 and τ_7 . By integrating out the D-term fixed modulus, we can determine the masses of light axions using an effective volume [38]

$$\mathcal{V} = \frac{1}{3} \left(\sqrt{\tau_s} \tau_b - \tau_7^{3/2} \right), \quad (3.16)$$

where $\tau_s \equiv \tau_1 - \tau_5$ and $\tau_b \equiv (10\tau_1 - \tau_5)/2$. The interplay between the non-perturbative effect and the leading order α' correction to the Kähler potential fixes $\sqrt{\tau_s}\tau_b$ and τ_7 according to the standard LVS approach. The non-perturbative effects on D_7 generate a potential for the axion c_7 , thereby giving a_7 a heavy mass and rendering it not the QCD axion. Then the two remaining massless axions are a_s and a_b , which remain massless due to the α' and g_s corrections. In the anisotropic limit $\tau_b \gg \tau_s \sim \tau_7$, the decay constants of the corresponding QCD axion and light ALP are given by [37]

$$\text{QCD axion: } f_{a_s} \simeq \frac{M_{\text{Pl}}}{4\pi\tau_s} \simeq 1 \times 10^{16} \text{ GeV}, \quad (3.17)$$

$$\text{ALP: } f_{a_b} \simeq \frac{M_{\text{Pl}}}{4\pi\tau_b} \simeq 5 \times 10^3 \text{ GeV}. \quad (3.18)$$

We can observe that the large decay constant of the axion a_s does not fall within the classic QCD axion window as depicted in eq. (1.1). However, its abundance can be diluted here through the late out-of-equilibrium decay of τ_7 and a_7 [36]. Furthermore, in this context, the abundance of the QCD axion can be naturally and significantly suppressed in the scenario involving mass mixing with the ALP, which we will discuss in the subsequent sections.

3.2.2 One QCD axion plus two ALPs

Here we introduce a model containing one QCD axion plus two ALPs from refs. [37, 39]. In contrast to the previous discussion, the QCD axion in this context possesses a decay constant with the intermediate-scale $\sim \mathcal{O}(10^{10})$ GeV.

The internal space of this model is an orientifold of a K3 or a T^4 fibred CY three-fold, characterized by specific Hodge numbers $h^{1,1} = h_+^{1,1} = 5$, realized as a hypersurface in a toric variety. The key divisors for modeling include the K3 or T^4 fiber D_1 , a divisor D_2 that controls the base of the fibration, a del Pezzo four-cycle D_3 , and two rigid divisors D_4 and D_5 . The Kähler form is given by [39]

$$J = t_1\hat{D}_1 + t_2\hat{D}_2 - t_3\hat{D}_3 - t_4\hat{D}_4 - t_5\hat{D}_5, \quad (3.19)$$

and the overall volume is

$$\mathcal{V} = \alpha \left[\sqrt{\tau_1}\tau_2 - \gamma_3\tau_3^{3/2} - \gamma_5\tau_5^{3/2} - \gamma_4(\tau_4 - x\tau_5)^{3/2} \right], \quad (3.20)$$

where α , γ_i , and x are constants of order one. The moduli-dependent FI terms result in a fixed combination of τ_4 and τ_5 at $\tau_5 = \lambda\hat{\tau}_4$, where $\lambda \equiv (x\gamma_4/\gamma_5)^2$ and $\hat{\tau}_4 \equiv \tau_4 - x\tau_5$. Then the four remaining Kähler moduli are τ_1 , τ_2 , τ_3 , and $\hat{\tau}_4$. After the D-term stabilization, we have the effective volume

$$\mathcal{V} = \alpha \left(\sqrt{\tau_1}\tau_2 - \gamma_3\tau_3^{3/2} - \lambda_4\hat{\tau}_4^{3/2} \right), \quad (3.21)$$

where $\lambda_4 \equiv \gamma_5 \lambda^{3/2} + \gamma_4$. The non-perturbative effects on D_3 generate a potential for the axion c_3 , thereby giving a_3 a heavy mass and rendering it not the QCD axion. The α' and g_s corrections result in the three remaining massless axions being a_1 , a_2 , and a_4 . The decay constant of the axion a_4 is given by [37]

$$\text{QCD axion: } f_{a_4} \simeq \frac{M_s}{\sqrt{4\pi}} \simeq 1 \times 10^{10} \text{ GeV}, \quad (3.22)$$

which is a perfect QCD axion candidate with an intermediate-scale decay constant. The axions a_1 and a_2 both belong to the light ALPs, and they can be discussed within the framework of two scenarios: isotropic and anisotropic. In the isotropic case $\tau_1 \sim \tau_2 \mathcal{V}^{2/3}$, the decay constants of a_1 and a_2 are given by

$$\text{ALPs: } f_{a_1} \simeq f_{a_2} \simeq \frac{M_{\text{Pl}}}{4\pi \mathcal{V}^{2/3}} \simeq 1 \times 10^8 \text{ GeV}. \quad (3.23)$$

While in the anisotropic case $\tau_2 \gg \tau_1 \sim \hat{\tau}_4$, the decay constants are given by

$$\text{ALPs: } f_{a_1} \simeq \frac{M_{\text{Pl}}}{4\pi \tau_1} \simeq 1 \times 10^{16} \text{ GeV}, \quad f_{a_2} \simeq \frac{M_{\text{Pl}}}{4\pi \tau_2} \simeq 5 \times 10^3 \text{ GeV}. \quad (3.24)$$

Notice that there is another anisotropic scenario, where the SM D7-stack wraps around the fiber divisor D_1 , featuring a_2 as the ALP and a_1 taking the role of the QCD axion. In this context, with the SM residing on D_1 , a_4 transforms into a heavy axion due to non-perturbative effects that are no longer canceled by the chiral intersection with SM matter fields.¹ In the subsequent discussions, we will focus only on the anisotropic scenario involving two ALPs presented in eq. (3.24).

3.2.3 One QCD axion plus multiple ALPs

In the previous two subsections, we introduced models containing one QCD axion plus one ALP and two ALPs, respectively. It is natural to extend this scenario to a model incorporating one QCD axion plus multiple ALPs. Here, we will provide only a brief overview of such an extension from ref. [37]. In this case, we require extra local cycles intersecting with visible branes, without imposing additional D-term conditions. Given n intersecting local cycles, of which d are fixed by D-terms, this leaves $n - d$ moduli frozen by loop corrections. Consequently, this results in $n - d$ light axions with intermediate-scale decay constants. For our purposes, in the subsequent sections, we will consider scenarios where the QCD axion and multiple ALPs have comparable decay constants, specifically with $f \sim \mathcal{O}(10^{10})$ GeV. In addition, there exist several explicit and globally consistent CY models, which feature one QCD axion and a small number of ALPs [103–105].

¹We are grateful to Michele Cicoli for clarifying this point.

Scenarios	f_{a_0} (GeV)	f_{A_1} (GeV)	f_{A_2} (GeV)	f_{A_N} (GeV)
1 + 1	1×10^{16}	5×10^3	—	—
1 + 2 (isotropic)	1×10^{10}	1×10^8	1×10^8	—
1 + 2 (anisotropic)	1×10^{10}	5×10^3	1×10^{16}	—
1 + N	$\sim 1 \times 10^{10}$			

Table 1: The decay constants of axions in the mixing scenarios originate from the type IIB string axiverse. Notice that, in the maximal $1 + N$ mixing scenario, the decay constants of all ALPs must simultaneously be either smaller than or larger than the decay constant of the QCD axion.

4 Axion mass mixing in the type IIB string axiverse

In this section, we investigate axion mass mixing in the type IIB string axiverse. Based on the above discussions, we will consider the following mixing scenarios here: $1 + 1$, $1 + 2$, and $1 + N$ ($N > 2$), where the number 1 preceding the plus sign indicates the quantity of the QCD axion, and the numbers following the plus sign represent the quantity of ALPs. Notice that the $1 + 2$ and $1 + N$ mixing scenarios considered here are proposed and studied for the first time. The decay constants of axions in the mixing scenarios, which originate from the type IIB string axiverse, are listed in table 1. Note also that the subscript “0” used hereinafter represents the QCD axion a_0 , whereas the subscript denoting a positive real number stands for the ALP A_i . It should not be confused with the subscripts employed in the previous sections.

4.1 The $1 + 1$ mixing scenario

Let us first discuss the so-called $1 + 1$ mixing scenario. To be honest, this is a common scenario that has garnered considerable attention and has been extensively studied in numerous pieces of previous literature. Consequently, there is nothing fundamentally new about this scenario in this subsection; however, it is still necessary to clarify it first within the context of the type IIB string axiverse [37–39]. Predominantly, this scenario focuses on the mass mixing that occurs between the QCD axion and an ALP, see e.g. refs. [49–51]. Furthermore, it is worth noting that scenarios involving the mixing between two QCD axions have also been given considerable consideration within the framework of this discussion, see also refs. [55, 75].

Considering the scenario presented in section 3.2.1 of the LVS axiverse, the decay constants of the QCD axion (a_0) and ALP (A_1) are given by

$$f_{a_0} = 1 \times 10^{16} \text{ GeV}, \quad f_{A_1} = 5 \times 10^3 \text{ GeV}. \quad (4.1)$$

The low-energy effective Lagrangian that describes this 1 + 1 mixing scenario can be formulated as follows

$$\begin{aligned} \mathcal{L} \supset & \frac{1}{2} f_{a_0}^2 (\partial\theta_0)^2 + \frac{1}{2} f_{A_1}^2 (\partial\Theta_1)^2 \\ & - m_{a_0}^2 f_{a_0}^2 [1 - \cos(n_{00}\theta_0 + n_{01}\Theta_1 + \delta_0)] \\ & - m_{A_1}^2 f_{A_1}^2 [1 - \cos(n_{10}\theta_0 + n_{11}\Theta_1 + \delta_1)] , \end{aligned} \quad (4.2)$$

where $\theta_0 = \phi_0/f_{a_0}$ and $\Theta_1 = \varphi_1/f_{A_1}$ represent the QCD axion and ALP angles, respectively, ϕ_0 and φ_1 are the QCD axion and ALP fields, m_{a_0} and m_{A_1} are the corresponding axion masses, n_{ij} are the domain wall numbers, and δ_i are the constant phases. Depending on the choice of domain wall numbers, this mixing scenario can be further categorized into the light QCD axion scenario and the heavy QCD axion scenario, which we will discuss in section 4.2.2. In this and subsequent discussions, we assume the constant phases to be zero, which can be seen as equivalent to demanding an independent solution for the strong CP problem. This assumption does not affect the evolution of axion fields during the mixing process and thus is justified within the context of our discussions. Notice that the single-field ALP is regarded as the most straightforward scenario, characterized by a constant mass m_{A_1} , whereas the QCD axion mass m_{a_0} is temperature-dependent, see also appendix C.

For our purpose, here the domain wall numbers n_{ij} should be taken as

$$n_{00} = 1, \quad n_{01} = 0, \quad n_{10} = 1, \quad n_{11} = 1. \quad (4.3)$$

To facilitate a more intuitive understanding, it is essential for us to define a matrix representing the domain wall numbers

$$\mathbf{n}_{2 \times 2} = \begin{pmatrix} 1 & 0 \\ 1 & 1 \end{pmatrix}. \quad (4.4)$$

Furthermore, the axion masses should be saturated by the relation

$$m_{A_1} < m_{a_0,0}, \quad (4.5)$$

where $m_{a_0,0}$ is the zero-temperature QCD axion mass. After substituting the mixing potential V_{mix} derived from eq. (4.2) into the equations of motion (EOMs), we obtain the following differential equations governing the evolution of axion fields

$$\ddot{\phi}_0 + 3H\dot{\phi}_0 + \frac{\partial V_{\text{mix}}(\phi_0, \varphi_1)}{\partial \phi_0} = 0, \quad (4.6)$$

$$\ddot{\varphi}_1 + 3H\dot{\varphi}_1 + \frac{\partial V_{\text{mix}}(\phi_0, \varphi_1)}{\partial \varphi_1} = 0, \quad (4.7)$$

where the dot notation denotes differentiation with respect to the physical time t (one dot for the first derivative and two dots for the second derivative), $\partial_{\phi_0} V_{\text{mix}}$ and $\partial_{\varphi_1} V_{\text{mix}}$ represent the partial derivatives of the mixing potential V_{mix} with respect to the axion fields, respectively, and $H(T)$ is the Hubble parameter. Specifically, for the fields ϕ_0 and φ_1 , the EOMs expand to

$$\ddot{\phi}_0 + 3H\dot{\phi}_0 + m_{a_0}^2 f_{a_0} \sin\left(\frac{\phi_0}{f_{a_0}}\right) + \frac{m_{A_1}^2 f_{A_1}^2}{f_{a_0}} \sin\left(\frac{\phi_0}{f_{a_0}} + \frac{\varphi_1}{f_{A_1}}\right) = 0, \quad (4.8)$$

$$\ddot{\varphi}_1 + 3H\dot{\varphi}_1 + m_{A_1}^2 f_{A_1} \sin\left(\frac{\phi_0}{f_{a_0}} + \frac{\varphi_1}{f_{A_1}}\right) = 0, \quad (4.9)$$

respectively. Assuming that the oscillation amplitudes of the axion field are significantly smaller than their respective decay constants, we can approximate the system and derive the mass mixing matrix within this model

$$\mathbf{M}^2 = \begin{pmatrix} m_{a_0}^2 + \frac{m_{A_1}^2 f_{A_1}^2}{f_{a_0}^2} & \frac{m_{A_1}^2 f_{A_1}}{f_{a_0}} \\ \frac{m_{A_1}^2 f_{A_1}}{f_{a_0}} & m_{A_1}^2 \end{pmatrix}. \quad (4.10)$$

By diagonalizing this matrix, we can identify the heavy and light mass eigenstates a_h and a_l , respectively, through the transformation

$$\begin{pmatrix} a_h \\ a_l \end{pmatrix} = \begin{pmatrix} \cos \alpha & \sin \alpha \\ -\sin \alpha & \cos \alpha \end{pmatrix} \begin{pmatrix} \phi_0 \\ \varphi_1 \end{pmatrix}, \quad (4.11)$$

where α is the mass mixing angle

$$\cos^2 \alpha = \frac{1}{2} \left(1 + \frac{m_{A_1}^2 - m_{a_0}^2 - \frac{m_{A_1}^2 f_{A_1}^2}{f_{a_0}^2}}{m_h^2 - m_l^2} \right), \quad (4.12)$$

and m_h and m_l (with the assumption that $m_h > m_l$) are the corresponding mass eigenvalues associated with the heavy and light mass eigenstates, respectively,

$$m_{h,l}^2 = \frac{1}{2} \left[m_{a_0}^2 + m_{A_1}^2 + \frac{m_{A_1}^2 f_{A_1}^2}{f_{a_0}^2} \right] \pm \frac{1}{2f_{a_0}^2} \left[-4m_{a_0}^2 m_{A_1}^2 f_{a_0}^4 + \left((m_{a_0}^2 + m_{A_1}^2) f_{a_0}^2 + m_{A_1}^2 f_{A_1}^2 \right)^2 \right]^{1/2}. \quad (4.13)$$

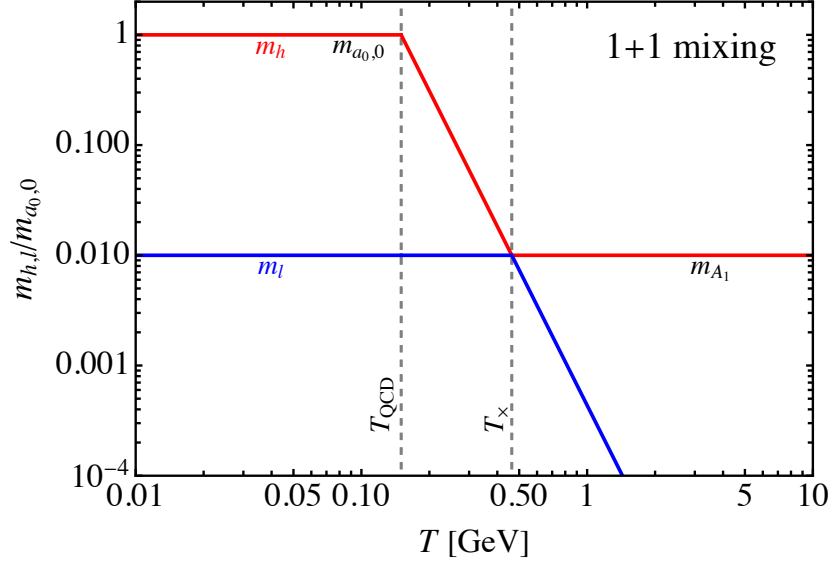


Figure 1: The illustration of the 1 + 1 mixing scenario. The solid lines represent the normalized temperature-dependent axion mass eigenvalues $m_h(T)$ and $m_l(T)$, respectively. The vertical gray lines (from right to left) indicate the temperatures T_{\times} and T_{QCD} , respectively. The masses $m_{a_0,0}$ and m_{A_1} are also labeled. The model parameters can be found in tables 1 and 2.

In figure 1, we provide a detailed depiction of the mass eigenvalues $m_{h,l}$. For comparison with the subsequent mixing scenarios, here we present the normalized eigenvalues $m_{h,l}/m_{a_0,0}$. It is noteworthy that a level crossing phenomenon may occur when the difference between the squared masses, denoted as $m_h^2 - m_l^2$, attains its minimal value. To determine the precise temperature at which this level crossing occurs within the mass mixing, we can solve the differential equation

$$\left. \frac{d(m_h^2(T) - m_l^2(T))}{dT} \right|_{T > T_{\text{QCD}}} = 0. \quad (4.14)$$

Upon solving this equation, we derive the level crossing temperature, T_{\times} , which is expressed as follows

$$T_{\times} = T_{\text{QCD}} \left(\frac{m_{a_0,0}^2 f_{a_0}^2}{m_{A_1}^2 (f_{a_0}^2 - f_{A_1}^2)} \right)^{\frac{1}{2b}}. \quad (4.15)$$

From this formula, we can also find that the condition $f_{a_0}^2 - f_{A_1}^2 > 0$ must be satisfied first. In this scenario, the evolution of axions is as follows. At high cosmic temperatures, the mass eigenvalues m_l and m_h are associated with the QCD axion a_0 and

Scenarios	r_{A_1}	r_{A_2}	r_{A_3}	\cdots	$r_{A_{N-1}}$	r_{A_N}
1 + 1	0.01	—	—		—	—
1 + 2 (isotropic)	0.0025	0.005	—		—	—
1 + 2 (anisotropic)	—	0.01	—		—	—
1 + N	0.001	0.003	0.009	\cdots	0.1	0.3

Table 2: The typical masses of ALPs in the mixing scenarios. Here we introduce the mass ratio r_{A_i} , which is defined as $r_{A_i} \equiv m_{A_i}/m_{a_0,0}$, where $m_{a_0,0}$ is the zero-temperature QCD axion mass.

the ALP A_1 , respectively. As the temperature gradually decreases towards T_x , a level crossing phenomenon occurs between the QCD axion and the ALP. Consequently, this level crossing results in m_l switching its association from the QCD axion to the ALP, while m_h correspondingly shifts its alignment from the ALP to the QCD axion. This sequential pattern of mixing continues as the temperature steadily declines. If the adiabatic condition is met, the axion energy density will undergo an adiabatic transfer at the level crossing [59, 63]. Notice also that this scenario can effectively suppress the QCD axion abundance and is therefore referred to as the light QCD axion scenario, see refs. [49, 51] for more details.

4.2 The 1 + 2 mixing scenario

In the subsequent subsections, our investigations into the scenario where the number of ALPs in the mass mixing exceeds one will be novel, constituting the first time such issues have been addressed.

4.2.1 Isotropic case

Considering the isotropic scenario presented in section 3.2.2 of the LVS axiverse, the decay constants of the QCD axion (a_0) and ALPs (A_1 and A_2) are given by

$$f_{a_0} = 1 \times 10^{10} \text{ GeV}, \quad f_{A_1} = 1 \times 10^8 \text{ GeV}, \quad f_{A_2} = 1 \times 10^8 \text{ GeV}. \quad (4.16)$$

Notice that the decay constants of both ALPs here are smaller than those of the QCD axion. The low-energy effective Lagrangian that describes this 1 + 2 mixing scenario can be formulated as follows

$$\begin{aligned} \mathcal{L} \supset & \frac{1}{2} f_{a_0}^2 (\partial\theta_0)^2 + \frac{1}{2} f_{A_1}^2 (\partial\Theta_1)^2 + \frac{1}{2} f_{A_2}^2 (\partial\Theta_2)^2 \\ & - m_{a_0}^2 f_{a_0}^2 [1 - \cos(n_{00}\theta + n_{01}\Theta_1 + n_{02}\Theta_2 + \delta_0)] \\ & - m_{A_1}^2 f_{A_1}^2 [1 - \cos(n_{10}\theta + n_{11}\Theta_1 + n_{12}\Theta_2 + \delta_1)] \\ & - m_{A_2}^2 f_{A_2}^2 [1 - \cos(n_{20}\theta + n_{21}\Theta_1 + n_{22}\Theta_2 + \delta_2)] , \end{aligned} \quad (4.17)$$

where $\Theta_1 = \varphi_1/f_{A_1}$ and $\Theta_2 = \varphi_2/f_{A_2}$ represent the ALP angles. Given that our focus is on the most straightforward scenario of the single-field ALP characterized by a constant mass, we find that, in circumstances involving axion mass mixing, the mixing process is confined to at most a single instance. Specifically, the QCD axion will mix with each individual ALP no more than once, and importantly, no mixing will take place among the ALPs themselves. This understanding is based on the assumption that we are dealing with the simplest form of ALP fields.

For our purpose, here the matrix of domain wall numbers should be taken as

$$\mathbf{n}_{3 \times 3} = \begin{pmatrix} 1 & 0 & 0 \\ 1 & 1 & 0 \\ 1 & 0 & 1 \end{pmatrix}. \quad (4.18)$$

Furthermore, the axion masses should be saturated by the relation

$$m_{A_1} < m_{a_0,0}, \quad m_{A_2} < m_{a_0,0}, \quad m_{A_1} \neq m_{A_2}. \quad (4.19)$$

Notice that, in order to more effectively demonstrate the intricacies of the mixing process, we hereby make the assumption that the masses of these two ALPs are unequal. In practical scenarios, if their masses were indeed identical, the mixing dynamics would be significantly simplified, leading to a mixing scenario with just one interaction; specifically, the QCD axion would mix solely with one of the ALPs, without the complexity of multiple mass-dependent interactions. Then the EOMs expand to

$$\begin{aligned} \ddot{\phi}_0 + 3H\dot{\phi}_0 + m_{a_0}^2 f_{a_0} \sin\left(\frac{\phi_0}{f_{a_0}}\right) + \frac{m_{A_1}^2 f_{A_1}^2}{f_{a_0}} \sin\left(\frac{\phi_0}{f_{a_0}} + \frac{\varphi_1}{f_{A_1}}\right) \\ + \frac{m_{A_2}^2 f_{A_2}^2}{f_{a_0}} \sin\left(\frac{\phi_0}{f_{a_0}} + \frac{\varphi_2}{f_{A_2}}\right) = 0, \end{aligned} \quad (4.20)$$

$$\ddot{\varphi}_1 + 3H\dot{\varphi}_1 + m_{A_1}^2 f_{A_1} \sin\left(\frac{\phi_0}{f_{a_0}} + \frac{\varphi_1}{f_{A_1}}\right) = 0, \quad (4.21)$$

$$\ddot{\varphi}_2 + 3H\dot{\varphi}_2 + m_{A_2}^2 f_{A_2} \sin\left(\frac{\phi_0}{f_{a_0}} + \frac{\varphi_2}{f_{A_2}}\right) = 0, \quad (4.22)$$

respectively. The mass mixing matrix is given by

$$\mathbf{M}^2 = \begin{pmatrix} m_{a_0}^2 + \frac{m_{A_1}^2 f_{A_1}^2 + m_{A_2}^2 f_{A_2}^2}{f_{a_0}^2} & \frac{m_{A_1}^2 f_{A_1}}{f_{a_0}} & \frac{m_{A_2}^2 f_{A_2}}{f_{a_0}} \\ \frac{m_{A_1}^2 f_{A_1}}{f_{a_0}} & m_{A_1}^2 & 0 \\ \frac{m_{A_2}^2 f_{A_2}}{f_{a_0}} & 0 & m_{A_2}^2 \end{pmatrix}. \quad (4.23)$$

As discussed earlier, since we are considering the mixing of the QCD axion with each ALP separately, the aforementioned mass mixing matrix can be expressed as the following effective mixing matrices

$$\mathbf{M}_1^2 = \begin{pmatrix} m_{a_0}^2 + \frac{m_{A_1}^2 f_{A_1}^2}{f_{a_0}^2} & \frac{m_{A_1}^2 f_{A_1}}{f_{a_0}} \\ \frac{m_{A_1}^2 f_{A_1}}{f_{a_0}} & m_{A_1}^2 \end{pmatrix}, \quad \mathbf{M}_2^2 = \begin{pmatrix} m_{a_0}^2 + \frac{m_{A_2}^2 f_{A_2}^2}{f_{a_0}^2} & \frac{m_{A_2}^2 f_{A_2}}{f_{a_0}} \\ \frac{m_{A_2}^2 f_{A_2}}{f_{a_0}} & m_{A_2}^2 \end{pmatrix}, \quad (4.24)$$

with the corresponding mass eigenvalues, respectively,

$$m_{h_1, l_1}^2 = \frac{1}{2} \left[m_{a_0}^2 + m_{A_1}^2 + \frac{m_{A_1}^2 f_{A_1}^2}{f_{a_0}^2} \right] \pm \frac{1}{2 f_{a_0}^2} \left[-4 m_{a_0}^2 m_{A_1}^2 f_{a_0}^4 + \left((m_{a_0}^2 + m_{A_1}^2) f_{a_0}^2 + m_{A_1}^2 f_{A_1}^2 \right)^2 \right]^{1/2}, \quad (4.25)$$

$$m_{h_2, l_2}^2 = \frac{1}{2} \left[m_{a_0}^2 + m_{A_2}^2 + \frac{m_{A_2}^2 f_{A_2}^2}{f_{a_0}^2} \right] \pm \frac{1}{2 f_{a_0}^2} \left[-4 m_{a_0}^2 m_{A_2}^2 f_{a_0}^4 + \left((m_{a_0}^2 + m_{A_2}^2) f_{a_0}^2 + m_{A_2}^2 f_{A_2}^2 \right)^2 \right]^{1/2}. \quad (4.26)$$

Based on eq. (4.19), if we consider a case where the mass of the ALP A_1 is smaller than that of A_2 ,

$$m_{A_1} < m_{A_2}, \quad (4.27)$$

the mass eigenvalues m_e can be expressed as

$$m_{e_1} = m_{h_2}, \quad (4.28)$$

$$m_{e_2} \simeq \begin{cases} m_{l_2}, & T \leq T_{\times}^{(m)} \\ m_{h_1}, & T > T_{\times}^{(m)} \end{cases} \quad (4.29)$$

$$m_{e_3} = m_{l_1}, \quad (4.30)$$

with

$$T_{\times 2} < T_{\times}^{(m)} < T_{\times 1}, \quad (4.31)$$

where $T_{\times}^{(m)}$ represents an intermediate temperature between the level crossing temperatures $T_{\times 1}$ and $T_{\times 2}$. In figure 2, we show the mass eigenvalues in this scenario, the red, blue, and purple solid lines correspond to the normalized eigenvalues m_{e_1} , m_{e_2} , and

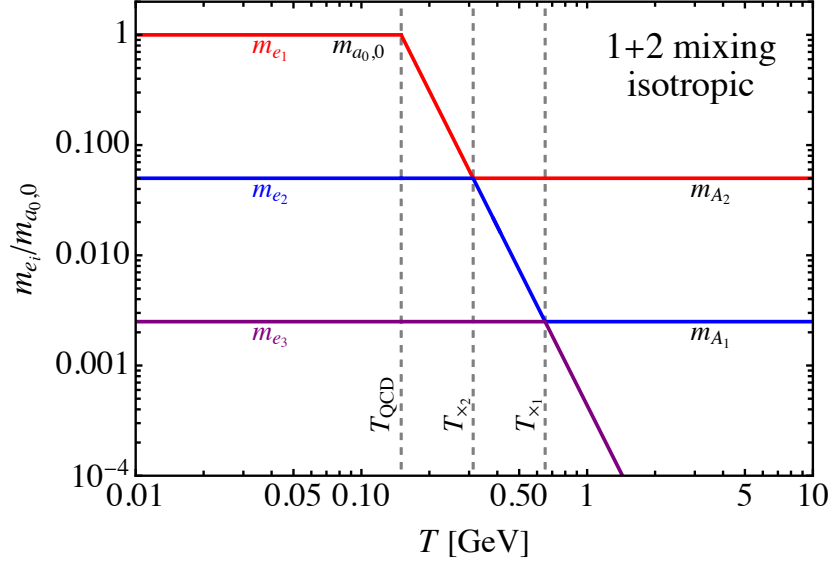


Figure 2: The illustration of the 1 + 2 mixing scenario (isotropic). The solid lines represent the normalized temperature-dependent axion mass eigenvalues $m_{e_1}(T)$, $m_{e_2}(T)$, and $m_{e_3}(T)$, respectively. The vertical gray lines (from right to left) indicate the temperatures T_{\times_1} , T_{\times_2} , and T_{QCD} , respectively. The masses $m_{a_0,0}$, m_{A_1} , and m_{A_2} are also labeled. The model parameters can be found in tables 1 and 2.

m_{e_3} , respectively. Here the level crossing temperatures can be obtained by solving the differential equations

$$\left. \frac{d(m_{e_2}^2(T) - m_{e_3}^2(T))}{dT} \right|_{T > T_{\times}^{(m)}} = 0, \quad (4.32)$$

$$\left. \frac{d(m_{e_1}^2(T) - m_{e_2}^2(T))}{dT} \right|_{T_{\text{QCD}} < T < T_{\times}^{(m)}} = 0, \quad (4.33)$$

then we have

$$T_{\times_1} = T_{\text{QCD}} \left(\frac{m_{a_0,0}^2 f_{a_0}^2}{m_{A_1}^2 (f_{a_0}^2 - f_{A_1}^2)} \right)^{\frac{1}{2b}}, \quad (4.34)$$

$$T_{\times_2} = T_{\text{QCD}} \left(\frac{m_{a_0,0}^2 f_{a_0}^2}{m_{A_2}^2 (f_{a_0}^2 - f_{A_2}^2)} \right)^{\frac{1}{2b}}. \quad (4.35)$$

We can find that T_{\times_1} is identical to the level crossing temperature presented in eq. (4.46). Note also that $T_{\times}^{(m)}$ is an estimated value, used to control a specific temperature range, and its exact value does not need to be determined. Subsequently, it is necessary to analyze the evolution of multiple axions in this scenario. At high cosmic temperatures, the mass eigenvalues m_{e_3} , m_{e_2} , and m_{e_1} are respectively associated with the QCD axion a_0 , the ALP A_1 , and the ALP A_2 . As the temperature decreases to T_{\times_1} , a level crossing occurs between the QCD axion and A_1 , resulting in m_{e_3} now corresponding to A_1 , and m_{e_2} shifting its correspondence to the QCD axion. As the temperature further descends to T_{\times_2} , another level crossing takes place, this time between the QCD axion and the ALP A_2 . Consequently, m_{e_2} now corresponds to A_2 , and m_{e_1} takes on the correspondence of the QCD axion. This sequence of mixings persists as the temperature continues to decline.

The interesting aspect we discover here is that m_{e_2} undergoes two transformations: initially corresponding to the ALP A_1 , then transitioning to the QCD axion a_0 , and ultimately to the ALP A_2 — a sequence that has never been observed before in the axion mass mixing. In a similar context, the double level crossings scenario exhibits a type of transition where, despite the occurrence of two sequential transformations, the axion ultimately reverts back to its initial state, as observed in ref. [51]. Conversely, in the scenario we are discussing, the axion initially aligns with one axion and ultimately with another distinct axion, highlighting a profound and essential distinction between these two scenarios. More importantly, our focus here is specifically on the mixing involving three distinct axions.

Additionally, we would like to point out an important aspect regarding the transition of axion energy density. In this 1 + 2 mixing scenario, we observe three transfer processes: first, the transfer from the QCD axion a_0 to the ALP A_1 ; second, the transfer from A_1 to a_0 , and subsequently from a_0 to the ALP A_2 ; and third, the transfer from A_2 to the QCD axion. This differs from the mutual transition between the QCD axion and ALP discussed in section 4.1.

4.2.2 Anisotropic case

Now, considering another anisotropic scenario presented in section 3.2.2 of the LVS axiverse, the decay constants of the QCD axion (a_0) and the two ALPs (A_1 and A_2) are given by

$$f_{a_0} = 1 \times 10^{10} \text{ GeV}, \quad f_{A_1} = 5 \times 10^3 \text{ GeV}, \quad f_{A_2} = 1 \times 10^{16} \text{ GeV}. \quad (4.36)$$

In contrast to section 4.2.1, the decay constants of the two ALPs presented here exhibit a variation, with one being smaller and the other being larger than those of the QCD

axion. Therefore, in this scenario, we consider the mixing involving either the QCD axion and the ALP A_1 , or the QCD axion and the ALP A_2 , rather than considering both simultaneously as was done in section 4.2.1. That is to say, in this case, the $1 + 2$ mixing scenario will transform into the $1 + 1$ mixing scenario.

Light QCD axion scenario Here, we first consider the mixing of the QCD axion and the ALP A_1 , with their decay constants

$$f_{a_0} = 1 \times 10^{10} \text{ GeV}, \quad f_{A_1} = 5 \times 10^3 \text{ GeV}. \quad (4.37)$$

One can find that the mass mixing in this scenario is identical to the $1 + 1$ mixing scenario discussed in section 4.1, therefore, we will not delve further into it here. This mixing is referred to as the light QCD axion scenario [49, 51]. Next, we will proceed to discuss an alternative, which is the heavy QCD axion scenario [50].

Heavy QCD axion scenario Then we discuss the mixing of the QCD axion and the ALP A_2 with their decay constants

$$f_{a_0} = 1 \times 10^{10} \text{ GeV}, \quad f_{A_2} = 1 \times 10^{16} \text{ GeV}. \quad (4.38)$$

The low-energy effective Lagrangian that describes this heavy QCD axion scenario can be formulated as follows

$$\begin{aligned} \mathcal{L} \supset & \frac{1}{2} f_{a_0}^2 (\partial\theta_0)^2 + \frac{1}{2} f_{A_2}^2 (\partial\Theta_2)^2 \\ & - m_{a_0}^2 f_{a_0}^2 [1 - \cos(n_{00}\theta_0 + n_{01}\Theta_2 + \delta_0)] \\ & - m_{A_2}^2 f_{A_2}^2 [1 - \cos(n_{20}\theta_0 + n_{21}\Theta_2 + \delta_2)]. \end{aligned} \quad (4.39)$$

For our purpose, here the matrix of domain wall numbers should be taken as

$$\mathbf{n}_{2 \times 2} = \begin{pmatrix} 1 & 1 \\ 0 & 1 \end{pmatrix}, \quad (4.40)$$

and the axion masses should be saturated by the relation

$$m_{A_1} < m_{a_0,0}. \quad (4.41)$$

The EOMs expand to

$$\ddot{\phi}_0 + 3H\dot{\phi}_0 + m_{a_0}^2 f_{a_0} \sin\left(\frac{\phi_0}{f_{a_0}} + \frac{\varphi_2}{f_{A_2}}\right) = 0, \quad (4.42)$$

$$\ddot{\varphi}_2 + 3H\dot{\varphi}_2 + m_{A_2}^2 f_{A_2} \sin\left(\frac{\varphi_2}{f_{A_2}}\right) + \frac{m_{a_0}^2 f_{a_0}}{f_{A_2}} \sin\left(\frac{\phi_0}{f_{a_0}} + \frac{\varphi_2}{f_{A_2}}\right) = 0, \quad (4.43)$$

respectively. The mass mixing matrix in this case is given by

$$\mathbf{M}^2 = \begin{pmatrix} m_{a_0}^2 & \frac{m_{a_0}^2 f_{a_0}}{f_{A_2}} \\ \frac{m_{a_0}^2 f_{a_0}}{f_{A_2}} & m_{A_2}^2 + \frac{m_{a_0}^2 f_{a_0}^2}{f_{A_2}^2} \end{pmatrix}, \quad (4.44)$$

with the mass eigenvalues

$$m_{h,l}^2 = \frac{1}{2} \left[m_{a_0}^2 + m_{A_2}^2 + \frac{m_{a_0}^2 f_{a_0}^2}{f_{A_2}^2} \right] \pm \frac{1}{2f_{A_2}^2} \left[-4m_{a_0}^2 m_{A_2}^2 f_{A_2}^4 + \left((m_{a_0}^2 + m_{A_2}^2) f_{A_2}^2 + m_{a_0}^2 f_{a_0}^2 \right)^2 \right]^{1/2}. \quad (4.45)$$

The level crossing temperature in this case is given by

$$T_\times = T_{\text{QCD}} \left(\frac{m_{a_0,0}^2 (f_{a_0}^2 + f_{A_2}^2)^2}{m_{A_2}^2 f_{A_2}^2 (f_{A_2}^2 - f_{a_0}^2)} \right)^{\frac{1}{2b}}. \quad (4.46)$$

Given that the fundamental nature of this particular scenario is a 1 + 1 mixing scenario, and the axion evolution process resembles that discussed in section 4.1, we will not delve into more here. In figure 3, we also show the mass eigenvalues in this scenario. It is worth noting that, unlike the light QCD axion scenario shown in section 4.1, this scenario effectively enhances the QCD axion abundance and is therefore referred to as the heavy QCD axion scenario. For a comprehensive understanding of this scenario and its applications, please refer to refs. [50, 106].

Looking back now at the mixing scenario presented in section 4.2.1, it is readily apparent that it corresponds to the light QCD axion scenario. If we consider the case where the decay constants of ALPs in section 4.2.1 are all larger than those of the QCD axion — that is, the heavy QCD axion scenario — then the matrix of domain wall numbers should be taken as

$$\mathbf{n}_{3 \times 3} = \begin{pmatrix} 1 & 1 & 1 \\ 0 & 1 & 0 \\ 0 & 0 & 1 \end{pmatrix}. \quad (4.47)$$

Here, we will not discuss further details about this scenario, but only present the mass mixing matrix

$$\mathbf{M}^2 = \begin{pmatrix} m_{a_0}^2 & \frac{m_{a_0}^2 f_{a_0}}{f_{A_1}} & \frac{m_{a_0}^2 f_{a_0}}{f_{A_2}} \\ \frac{m_{a_0}^2 f_{a_0}}{f_{A_1}} & m_{A_1}^2 + \frac{m_{a_0}^2 f_{a_0}^2}{f_{A_1}^2} & \frac{m_{a_0}^2 f_{a_0}}{f_{A_1} f_{A_2}} \\ \frac{m_{a_0}^2 f_{a_0}}{f_{A_2}} & \frac{m_{a_0}^2 f_{a_0}}{f_{A_1} f_{A_2}} & m_{A_2}^2 + \frac{m_{a_0}^2 f_{a_0}^2}{f_{A_2}^2} \end{pmatrix}, \quad (4.48)$$

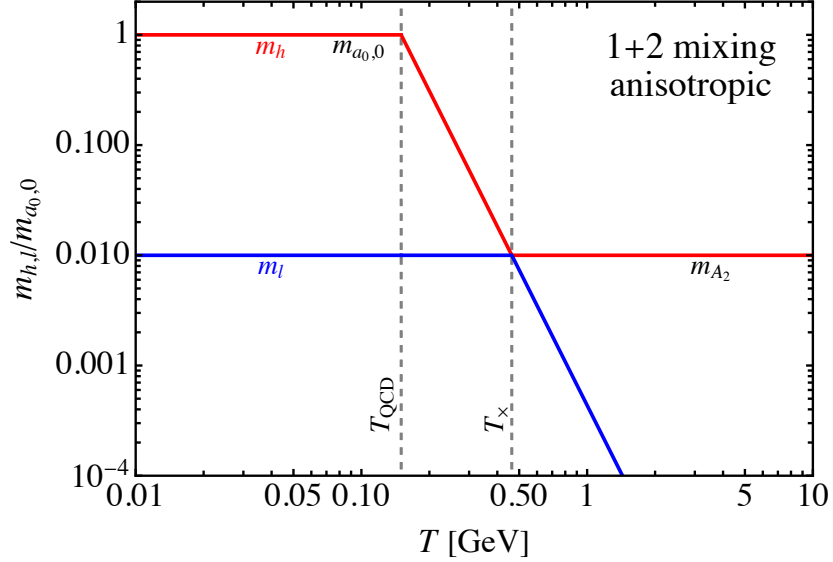


Figure 3: The illustration of the 1 + 2 mixing scenario (anisotropic). The solid lines represent the normalized temperature-dependent axion mass eigenvalues $m_h(T)$ and $m_l(T)$, respectively. The model parameters can be found in tables 1 and 2. Notice that this is actually a 1 + 1 mixing scenario.

with the effective mixing matrices

$$\mathbf{M}_1^2 = \begin{pmatrix} m_{a_0}^2 & \frac{m_{a_0}^2 f_{a_0}}{f_{A_1}} \\ \frac{m_{a_0}^2 f_{a_0}}{f_{A_1}} & m_{A_1}^2 + \frac{m_{a_0}^2 f_{a_0}^2}{f_{A_1}^2} \end{pmatrix}, \quad \mathbf{M}_2^2 = \begin{pmatrix} m_{a_0}^2 & \frac{m_{a_0}^2 f_{a_0}}{f_{A_2}} \\ \frac{m_{a_0}^2 f_{a_0}}{f_{A_2}} & m_{A_2}^2 + \frac{m_{a_0}^2 f_{a_0}^2}{f_{A_2}^2} \end{pmatrix}. \quad (4.49)$$

4.3 The 1 + N mixing scenario

In this subsection, we will generalize the previously discussed 1 + 2 mixing scenario to the 1 + N ($N > 2$) mixing scenario.

Now, considering the scenario presented in section 3.2.3 of the LVS axiverse, the decay constants of the QCD axion (a_0) and the multiple ALPs (A_i), numbered N , can be approximately given by

$$f_{a_0} \sim f_{A_i} \sim 1 \times 10^{10} \text{ GeV}. \quad (4.50)$$

Here we first discuss the scenario where the decay constants of ALPs are all smaller than those of the QCD axion,

$$f_{A_i} < f_{a_0}, \forall i. \quad (4.51)$$

The low-energy effective Lagrangian that describes this $1 + N$ mixing scenario can be formulated as follows

$$\begin{aligned}
\mathcal{L} \supset & \frac{1}{2} f_{a_0}^2 (\partial\theta_0)^2 + \frac{1}{2} \sum_{i=1}^N f_{A_i}^2 (\partial\Theta_i)^2 \\
& - m_{a_0}^2 f_{a_0}^2 \left[1 - \cos \left(n_{00}\theta_0 + \sum_{j=1}^N n_{0j}\Theta_j + \delta_0 \right) \right] \\
& - \sum_{i=1}^N m_{A_i}^2 f_{A_i}^2 \left[1 - \cos \left(n_{i0}\theta_0 + \sum_{j=1}^N n_{ij}\Theta_j + \delta_i \right) \right],
\end{aligned} \tag{4.52}$$

where $\Theta_i = \varphi_i/f_{A_i}$ are the ALP angles, φ_i represent the ALP fields, f_{A_i} and m_{A_i} are the ALP decay constants and masses, respectively.

For our purpose, here the matrix of domain wall numbers should be taken as

$$\mathbf{n}_{(N+1)\times(N+1)} = \begin{pmatrix} 1 & 0 & 0 & 0 & \cdots & 0 \\ 1 & 1 & 0 & 0 & \cdots & 0 \\ 1 & 0 & 1 & 0 & \cdots & 0 \\ 1 & 0 & 0 & 1 & \cdots & 0 \\ \vdots & \vdots & \vdots & \vdots & \ddots & \vdots \\ 1 & 0 & 0 & 0 & \cdots & 1 \end{pmatrix}, \tag{4.53}$$

and the axion masses should be saturated by the relation

$$m_{A_i} < m_{a_0,0}, \forall i, \quad m_{A_i} \neq m_{A_j}, \forall i \neq j. \tag{4.54}$$

Then the EOMs expand to

$$\ddot{\phi}_0 + 3H\dot{\phi}_0 + m_{a_0}^2 f_{a_0} \sin\left(\frac{\phi_0}{f_{a_0}}\right) + \sum_{i=1}^N \frac{m_{A_i}^2 f_{A_i}^2}{f_{a_0}} \sin\left(\frac{\phi_0}{f_{a_0}} + \frac{\varphi_i}{f_{A_i}}\right) = 0, \tag{4.55}$$

$$\ddot{\varphi}_1 + 3H\dot{\varphi}_1 + m_{A_1}^2 f_{A_1} \sin\left(\frac{\phi_0}{f_{a_0}} + \frac{\varphi_1}{f_{A_1}}\right) = 0, \tag{4.56}$$

$$\ddot{\varphi}_2 + 3H\dot{\varphi}_2 + m_{A_2}^2 f_{A_2} \sin\left(\frac{\phi_0}{f_{a_0}} + \frac{\varphi_2}{f_{A_2}}\right) = 0, \tag{4.57}$$

\vdots

$$\ddot{\varphi}_N + 3H\dot{\varphi}_N + m_{A_N}^2 f_{A_N} \sin\left(\frac{\phi_0}{f_{a_0}} + \frac{\varphi_N}{f_{A_N}}\right) = 0, \tag{4.58}$$

respectively, with the mass mixing matrix

$$\mathbf{M}^2 = \begin{pmatrix} m_{a_0}^2 + \frac{1}{f_{a_0}^2} \sum_{i=1}^N m_{A_i}^2 f_{A_i}^2 & \frac{m_{A_1}^2 f_{A_1}}{f_{a_0}} & \frac{m_{A_2}^2 f_{A_2}}{f_{a_0}} & \cdots & \frac{m_{A_N}^2 f_{A_N}}{f_{a_0}} \\ \frac{m_{A_1}^2 f_{A_1}}{f_{a_0}} & m_{A_1}^2 & 0 & \cdots & 0 \\ \frac{m_{A_2}^2 f_{A_2}}{f_{a_0}} & 0 & m_{A_2}^2 & \cdots & 0 \\ \vdots & \vdots & \vdots & \ddots & \vdots \\ \frac{m_{A_N}^2 f_{A_N}}{f_{a_0}} & 0 & 0 & \cdots & m_{A_N}^2 \end{pmatrix}. \quad (4.59)$$

As discussed earlier, the effective mixing matrices here can be separately expressed as

$$\mathbf{M}_i^2 = \begin{pmatrix} m_{a_0}^2 + \frac{m_{A_i}^2 f_{A_i}^2}{f_{a_0}^2} & \frac{m_{A_i}^2 f_{A_i}}{f_{a_0}} \\ \frac{m_{A_i}^2 f_{A_i}}{f_{a_0}} & m_{A_i}^2 \end{pmatrix}, \quad (4.60)$$

with the corresponding mass eigenvalues

$$m_{h_i, l_i}^2 = \frac{1}{2} \left[m_{a_0}^2 + m_{A_i}^2 + \frac{m_{A_i}^2 f_{A_i}^2}{f_{a_0}^2} \right] \pm \frac{1}{2f_{a_0}^2} \left[-4m_{a_0}^2 m_{A_i}^2 f_{a_0}^4 + \left((m_{a_0}^2 + m_{A_i}^2) f_{a_0}^2 + m_{A_i}^2 f_{A_i}^2 \right)^2 \right]^{1/2}. \quad (4.61)$$

If we consider a case where the mass of A_i is smaller than that of A_{i+1} ,

$$m_{A_1} < m_{A_2} < \cdots < m_{A_N}, \quad (4.62)$$

the mass eigenvalues m_{e_i} can be expressed as

$$m_{e_1} = m_{h_N}, \quad (4.63)$$

$$m_{e_2} \simeq \begin{cases} m_{l_N}, & T \leq T_{\times N-1}^{(m)} \\ m_{h_{N-1}}, & T > T_{\times N-1}^{(m)} \end{cases} \quad (4.64)$$

$$m_{e_3} \simeq \begin{cases} m_{l_{N-1}}, & T \leq T_{\times N-2}^{(m)} \\ m_{h_{N-2}}, & T > T_{\times N-2}^{(m)} \end{cases} \quad (4.65)$$

\vdots

$$m_{e_N} \simeq \begin{cases} m_{l_2}, & T \leq T_{\times 1}^{(m)} \\ m_{h_1}, & T > T_{\times 1}^{(m)} \end{cases} \quad (4.66)$$

$$m_{e_{N+1}} = m_{l_1}, \quad (4.67)$$

with

$$T_{\times_{i+1}} < T_{\times_i}^{(m)} < T_{\times_i}, \quad (4.68)$$

where $T_{\times_i}^{(m)}$ represent the corresponding intermediate temperatures. In this case, the level crossing temperatures T_{\times_i} can be obtained by solving the differential equations

$$\left. \frac{d \left(m_{e_N}^2(T) - m_{e_{N+1}}^2(T) \right)}{dT} \right|_{T > T_{\times_1}^{(m)}} = 0, \quad i = 1 \quad (4.69)$$

$$\left. \frac{d \left(m_{e_{N-i+1}}^2(T) - m_{e_{N-i+2}}^2(T) \right)}{dT} \right|_{T_{\times_i}^{(m)} < T < T_{\times_{i-1}}^{(m)}} = 0, \quad 1 < i < N \quad (4.70)$$

$$\left. \frac{d \left(m_{e_1}^2(T) - m_{e_2}^2(T) \right)}{dT} \right|_{T_{\text{QCD}} < T < T_{\times_{N-1}}^{(m)}} = 0, \quad i = N \quad (4.71)$$

then we have

$$T_{\times_i} = T_{\text{QCD}} \left(\frac{m_{a_0,0}^2 f_{a_0}^2}{m_{A_i}^2 (f_{a_0}^2 - f_{A_i}^2)} \right)^{\frac{1}{2b}}. \quad (4.72)$$

In figure 4, we show the mass eigenvalues in this scenario, the solid lines correspond to the normalized m_{e_i} . We can observe that the evolution process of axions here is similar to that described in section 4.2.1, except for the significantly greater number of ALPs involved here, leading to multiple level crossings. Notice that in this figure, the decay constants for all ALPs have been assumed to be identical. Furthermore, these decay constants are not significantly smaller than those of the QCD axion, in contrast to the scenarios depicted in figures 1 and 2. Consequently, the level crossing phenomenon demonstrated here is more pronounced.

Here we summarize and delineate two key conditions that are essential for the occurrence of maximal mixing among multiple axion mass eigenstates. Firstly, the masses of all ALPs must be strictly smaller than the zero-temperature mass of the QCD axion. Furthermore, it is crucial to note that there should be no equivalence in the masses of any two ALPs; rather, they should exhibit a distinct hierarchy among themselves. This hierarchical distribution ensures that no two ALPs can interfere with each other's mixing dynamics, thereby facilitating maximal mixing. Secondly, the decay constants of all ALPs play a crucial role in determining the extent of maximal mixing. Specifically, it is necessary that the decay constants of all ALPs must uniformly be either smaller than or larger than the decay constant of the QCD axion. In this

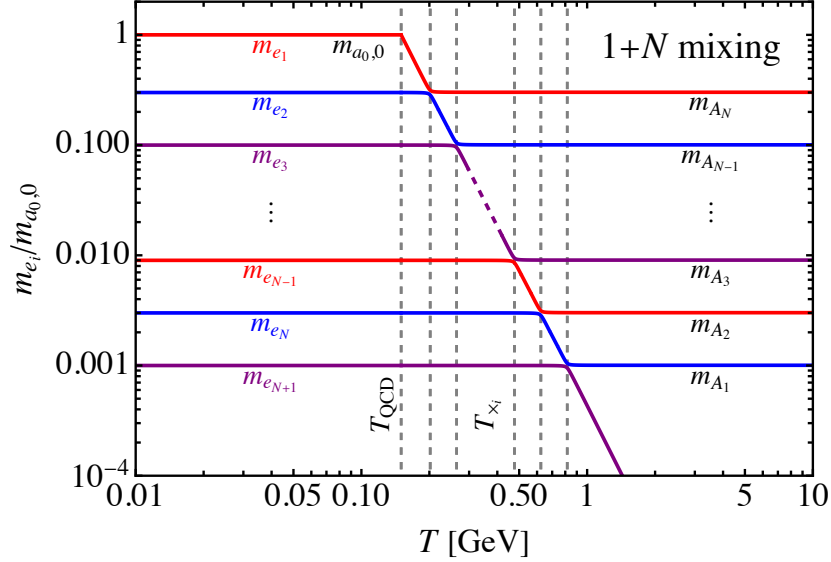


Figure 4: The illustration of the $1 + N$ mixing scenario. The solid lines represent the normalized temperature-dependent axion mass eigenvalues $m_{e_i}(T)$, respectively. The vertical gray lines (from right to left) indicate the temperatures T_{\times_i} and T_{QCD} , respectively. The masses $m_{a_0,0}$ and m_{A_i} are also labeled. Here we set $f_{a_0} = 1 \times 10^{10}$ GeV and $f_{A_i} = 1 \times 10^9$ GeV. The other model parameters can be found in table 2.

context, smaller corresponds to the light QCD axion scenario, while larger corresponds to the heavy QCD axion scenario. Any deviation from this condition, where some decay constants are smaller and others are larger, would inevitably compromise the maximal mixing. As described in section 4.2.2, the anisotropic $1 + 2$ mixing scenario can be transformed into two $1 + 1$ mixing scenarios, which respectively correspond to the light and heavy QCD axion scenarios. Therefore, by adhering to these two stringent conditions, we can ensure the occurrence of maximal mixing among multiple axion mass eigenstates.

Furthermore, in conjunction with our previous discussions, it is crucial to highlight a significant aspect regarding the transition of axion energy density:

- *The energy transfer ultimately takes place solely between the two axions that possess the closest masses.*

In the context of the $1 + N$ mixing scenario, we observe the transfer processes: first, the transfer from the QCD axion a_0 to the ALP A_1 ; second, the transfer from A_1 to a_0 , and subsequently from a_0 to the ALP A_2 ; third, the transfer from A_2 to a_0 , and subsequently from a_0 to A_3 ; \dots ; and finally, the transfer from A_N to the QCD axion. This is an extension of the $1 + 2$ mixing scenario presented in section 4.2.1 and differs

from the 1 + 1 mixing scenario discussed in section 4.1. However, the discussion in section 4.1 aligns with our conclusion here, which is that axion energy density transfer only occurs between the two axions with the closest masses.

4.3.1 Heavy QCD axion scenario

The above discussions focus on the light QCD axion scenario. In addition, if we consider the heavy QCD axion scenario where the decay constants of ALPs are all larger than those of the QCD axion,

$$f_{A_i} > f_{a_0}, \forall i, \quad (4.73)$$

then the matrix of domain wall numbers should be taken as

$$\mathbf{n}_{(N+1) \times (N+1)} = \begin{pmatrix} 1 & 1 & 1 & 1 & \cdots & 1 \\ 0 & 1 & 0 & 0 & \cdots & 0 \\ 0 & 0 & 1 & 0 & \cdots & 0 \\ 0 & 0 & 0 & 1 & \cdots & 0 \\ \vdots & \vdots & \vdots & \vdots & \ddots & \vdots \\ 0 & 0 & 0 & 0 & \cdots & 1 \end{pmatrix}, \quad (4.74)$$

and the mass mixing matrix is given by

$$\mathbf{M}^2 = \begin{pmatrix} m_{a_0}^2 & \frac{m_{a_0}^2 f_{a_0}}{f_{A_1}} & \frac{m_{a_0}^2 f_{a_0}}{f_{A_2}} & \cdots & \frac{m_{a_0}^2 f_{a_0}}{f_{A_N}} \\ \frac{m_{a_0}^2 f_{a_0}}{f_{A_1}} & m_{A_1}^2 + \frac{m_{a_0}^2 f_{a_0}^2}{f_{A_1}^2} & \frac{m_{a_0}^2 f_{a_0}^2}{f_{A_1} f_{A_2}} & \cdots & \frac{m_{a_0}^2 f_{a_0}^2}{f_{A_1} f_{A_N}} \\ \frac{m_{a_0}^2 f_{a_0}}{f_{A_2}} & \frac{m_{a_0}^2 f_{a_0}^2}{f_{A_1} f_{A_2}} & m_{A_2}^2 + \frac{m_{a_0}^2 f_{a_0}^2}{f_{A_2}^2} & \cdots & \frac{m_{a_0}^2 f_{a_0}^2}{f_{A_2} f_{A_N}} \\ \vdots & \vdots & \vdots & \ddots & \vdots \\ \frac{m_{a_0}^2 f_{a_0}}{f_{A_N}} & \frac{m_{a_0}^2 f_{a_0}^2}{f_{A_1} f_{A_N}} & \frac{m_{a_0}^2 f_{a_0}^2}{f_{A_2} f_{A_N}} & \cdots & m_{A_N}^2 + \frac{m_{a_0}^2 f_{a_0}^2}{f_{A_N}^2} \end{pmatrix}, \quad (4.75)$$

with the effective mixing matrices

$$\mathbf{M}_i^2 = \begin{pmatrix} m_{a_0}^2 & \frac{m_{a_0}^2 f_{a_0}}{f_{A_i}} \\ \frac{m_{a_0}^2 f_{a_0}}{f_{A_i}} & m_{A_i}^2 + \frac{m_{a_0}^2 f_{a_0}^2}{f_{A_i}^2} \end{pmatrix}. \quad (4.76)$$

Notice that the relation eq. (4.54) should also be saturated here. Further details regarding this heavy QCD axion scenario will not be discussed in detail in this context.

In comparison to the aforementioned discussions, it is predictable that the evolution of axions under this particular scenario will not undergo significant deviations. Nevertheless, the modifications in axion energy density will be substantial and worth paying attention to.

5 Cosmological implications

In this section, we briefly discuss the potential cosmological implications of axion mass mixing in the string axiverse, including axion relic density, isocurvature fluctuations, dark energy, domain walls, gravitational waves, and also primordial black holes. Notice that this is only a brief overview of these cosmological effects mentioned above, intended to give readers a general understanding. More detailed discussions would require analysis based on specific models and are thus not further elaborated upon in this context.

5.1 Dark matter

The most immediate effect of axion mass mixing is on the abundance of axion dark matter, a topic that has been extensively discussed in previous literature concerning the two-axion mixing [59–63]. As we mentioned earlier, based on their impact on the relic density of the QCD axion, different types of axion mass mixing can be categorized into the light QCD axion scenario [49, 51] and the heavy QCD axion scenario [50]. Notice that this classification also applies to the ALP dark matter as well as to mixing scenarios involving more than two axions.

Specifically, in the LVS axiverse, the QCD axion with a higher-scale decay constant can be diluted by the late out-of-equilibrium decay of some heavy moduli [36]. Within this framework, the overproduction and underproduction of dark matter abundance of the QCD axion (or ALPs) can be naturally accounted for through their mass mixing. As an example, let us discuss the abundance of QCD axion dark matter in the 1+2 mixing scenario where eq. (4.18) is adopted.² For simplicity, we consider the pre-inflationary scenario where the PQ symmetry is spontaneously broken during inflation, and the axion energy density transfers at the level crossing temperatures T_{\times_i} are adiabatic. As shown in figure 2, we observe three axion energy density transfer processes: first, the transfer from the QCD axion a_0 to the ALP A_1 ; second, the transfer from A_1 to a_0 , and subsequently from a_0 to the ALP A_2 ; and third, the transfer from A_2 to the QCD axion. Therefore, to determine the relic density of the QCD axion, we need to start

²For an example concerning the axion dark matter abundance in a 1 + 1 mixing scenario, please refer to recent refs. [62, 63].

with the ALP A_2 , whose initial energy density at the oscillation temperature T_{osc,A_2} is given by

$$\rho_{A_2,\text{osc}} = \frac{1}{2} m_{A_2}^2 f_{A_2}^2 \Theta_{i,A_2}^2, \quad (5.1)$$

where Θ_{i,A_2} is the initial misalignment angle of A_2 . Then at $T_{\times_2} < T < T_{\text{osc},A_2}$, the energy density of A_2 is adiabatic invariant. At the level crossing temperature T_{\times_2} , this energy density can be described by

$$\rho_{A_2,\times_2} = \frac{1}{2} m_{A_2}^2 f_{A_2}^2 \Theta_{i,A_2}^2 \left(\frac{\mathbf{a}_{\text{osc},A_2}}{\mathbf{a}_{\times_2}} \right)^3, \quad (5.2)$$

where $\mathbf{a}_{\text{osc},A_2}$ and \mathbf{a}_{\times_2} are the scale factors at T_{osc,A_2} and T_{\times_2} , respectively. Subsequently, the ρ_{A_2,\times_2} is transferred to the QCD axion, and the axion energy density is adiabatic invariant until the current cosmic microwave background (CMB) temperature T_0 . Consequently, we obtain the present QCD axion energy density

$$\rho_{a_0,0} = \frac{1}{2} m_{a_0,0} m_{A_2} f_{A_2}^2 \Theta_{i,A_2}^2 \left(\frac{\mathbf{a}_{\text{osc},A_2}}{\mathbf{a}_0} \right)^3, \quad (5.3)$$

where \mathbf{a}_0 is the scale factor today. Compared with the no mass mixing case (see also appendix C), the QCD axion relic density can be effectively suppressed as

$$\sim \left(\frac{m_{a_0,\text{osc}}}{m_{A_2}} \right)^{1/2} \left(\frac{f_{A_2}}{f_{a_0}} \right)^2 \ll 1, \quad (5.4)$$

where $m_{a_0,\text{osc}}$ corresponds to the QCD axion mass at the oscillation temperature T_{osc,a_0} . Although this formula appears similar to eq. (3.26) in a 1 + 1 mixing scenario presented in ref. [62], it fundamentally differs from the mutual transfer between the QCD axion and ALP in that two-axion scenario. Note that this relates to the light QCD axion scenario, which is valid when the QCD axion has a higher-scale decay constant. If the matrix of domain wall numbers outlined in eq. (4.47) is adopted, corresponding to the heavy QCD axion scenario, the QCD axion abundance can be enhanced as

$$\sim \left(\frac{m_{a_0,\text{osc}}}{m_{A_2}} \right)^{1/2} \left(\frac{f_{A_2}}{f_{a_0}} \right)^2 \gtrsim 1, \quad (5.5)$$

where $f_{A_2} > f_{a_0}$. In addition, when extending the 1 + 2 mixing scenario to the more general 1 + N scenario, we find that the abundance of the QCD axion depends only on the ALP with the largest mass in the maximal mixing as

$$\sim \left(\frac{m_{a_0,\text{osc}}}{m_{A_N}} \right)^{1/2} \left(\frac{f_{A_N}}{f_{a_0}} \right)^2, \quad (5.6)$$

where eq. (4.62) is adopted in this scenario. Lastly, the discussion on the abundance of ALPs can also be analyzed using a similar method mentioned above, and thus will not be elaborated further here.

5.2 Isocurvature fluctuations

Subsequently, another notable effect of axion mass mixing is its impact on isocurvature fluctuations, with scenarios involving the mixing of two axions having been discussed in previous literature [49, 64]. If the PQ symmetry is broken during inflation, the QCD axion will acquire quantum fluctuations, which leads to scale-invariant cold dark matter isocurvature density perturbations imprinted on the CMB temperature anisotropy. Similarly, ALPs can also generate isocurvature perturbations. The amount of isocurvature perturbations is stringently constrained by the CMB observations [107, 108].

Considering the multi-axion system, the quantum fluctuations of the QCD axion and ALPs are given by

$$\delta\theta_i = \frac{H_I}{2\pi f_{a_0}}, \quad \delta\Theta_{i,A_i} = \frac{H_I}{2\pi f_{A_i}}, \quad (5.7)$$

where H_I is the Hubble parameter during inflation. Consequently, the dark matter isocurvature perturbation can be described by

$$\Delta_{S,DM} = \left(\frac{\Omega_{\text{tot}}}{\Omega_{\text{DM}}} \right) \Delta_{S,\text{axion}}, \quad (5.8)$$

with

$$\Omega_{\text{tot}} = \Omega_{a_0} + \sum_{i=1}^N \Omega_{A_i}, \quad (5.9)$$

where Ω_{tot} and Ω_{DM} are the density parameters for the total axions and the observed dark matter, respectively. The power spectrum $\Delta_{S,\text{axion}}^2$ is given by

$$\Delta_{S,\text{axion}}^2 = \left(\frac{\partial \ln \Omega_{\text{tot}}}{\partial \theta_i} \right)^2 \left(\frac{H_I}{2\pi f_{a_0}} \right)^2 + \sum_{i=1}^N \left(\frac{\partial \ln \Omega_{\text{tot}}}{\partial \Theta_{i,A_i}} \right)^2 \left(\frac{H_I}{2\pi f_{A_i}} \right)^2, \quad (5.10)$$

which can be rewritten as

$$\left| \frac{\Delta_{S,\text{axion}}}{\delta\theta_i} \right|^2 = \left(\frac{\partial \ln \Omega_{\text{tot}}}{\partial \theta_i} \right)^2 + \sum_{i=1}^N \left(\frac{\partial \ln \Omega_{\text{tot}}}{\partial \Theta_{i,A_i}} \right)^2 \left(\frac{f_{a_0}}{f_{A_i}} \right)^2. \quad (5.11)$$

Due to the presence of mass mixing, the abundance of axions is no longer solely dependent on the initial misalignment angle, but also on the mass ratio among these axions. As a result, the isocurvature perturbations of axions can be effectively altered. Furthermore, under certain specific conditions, as illustrated in a case of two-axion mixing in ref. [64], they can be effectively suppressed.

5.3 Dark energy

Furthermore, the effect of axion mass mixing also has a potential impact on the composition of dark energy. Recently, a case of two-axion mixing was investigated in refs. [65, 66]. Considering that ALP dominates the cosmological energy density and acts as dark energy, to achieve the observed dark energy amount, the number density of ALP needs to be enhanced through a specific mechanism. Assuming the QCD axion comprises the dark matter, a non-adiabatic level crossing between the QCD axion and ALP shortly before the matter-dark energy equality may convert a small fraction of dark matter into dark energy. At the level crossing, in order to reach the matter-dark energy equality at $z_{\text{DE}} \sim 5$, the ratio of dark energy density to matter density is required to be approximately [65]

$$\frac{\rho_{\text{DE}}}{\rho_m} \Big|_{T=T_\times} = \left(\frac{1 + z_{\text{DE}}}{1 + z_\times} \right)^3 \sim 1\% - 2\%, \quad (5.12)$$

where z represents the redshift. This process provides a mechanism for boosting the number density of ALP and thus addresses this issue.

We predict that this mechanism will also be applicable to the $1+2$ mixing scenario, and furthermore, to the $1+N$ mixing scenario that we discussed previously. However, given that the number of ALPs will be more than one in these cases, the specific effects are still unclear and require further exploration.

5.4 Domain walls

The formation of domain walls due to the two-axion mixing has been investigated in refs. [67–69]. In this scenario, axion oscillations begin shortly before the level crossing temperature. If the initial energy density is sufficient to overcome the potential barrier, axion dynamics exhibits chaotic behavior, potentially leading to the formation of domain walls. Since cosmic strings do not form in this context, these domain walls remain stable on a cosmological scale in their absence.

Given that domain walls evolve more slowly with cosmic expansion compared to radiation or matter, they will ultimately come to dominate the Universe, contradicting the standard cosmology. Therefore, to prevent the domain wall problem, they must annihilate before achieving dominance. Typically, a slight energy difference between different vacua can be introduced to facilitate the annihilation of domain walls. However, in the mixing scenario, the domain walls will naturally become unstable and annihilate due to an inherent bias term. Specifically, the evolution of domain walls over time can be expressed as [109–112]

$$\rho_{\text{wall}}(t) = \mathcal{A} \frac{\sigma_{\text{wall}}}{t}, \quad (5.13)$$

where \mathcal{A} represents the scaling parameter and σ_{wall} represents the tension of domain walls. The annihilation of domain walls becomes significant when the tension pressure $p_T \simeq \rho_{\text{wall}}$ is comparable to the volume pressure $p_V \simeq \Lambda_b^4$, then we have

$$\mathcal{A} \frac{\sigma_{\text{wall}}}{t_{\text{ann}}} \simeq \Lambda_b^4, \quad (5.14)$$

where Λ_b is a bias parameter and t_{ann} is the domain walls annihilation time. Notice that when considering the mixing in scenarios involving more than two axions, the aforementioned discussions about the formation of domain walls may become relatively complicated. Additionally, the annihilation of domain walls should occur before the Big Bang Nucleosynthesis (BBN) epoch to avoid stringent constraints.

5.5 Gravitational waves

It is natural to consider the gravitational waves emitted by the annihilation of the aforementioned domain walls, which have also been extensively discussed in the literature [69–73]. In this case, the gravitational waves can be characterized by their peak frequency f_p and peak amplitude $\Omega_{\text{GW}}(t)_p$. The peak frequency corresponds to the Hubble parameter at the time of annihilation and is redshifted due to the cosmic expansion. The present peak frequency depends on several parameters, including the domain walls tension and energy scales. The peak amplitude of gravitational waves at the annihilation time is given by a formula involving the domain walls tension and the efficiency parameter. The present peak amplitude is then calculated, taking into account the change in the number of effective degrees of freedom. Finally, the present gravitational waves spectrum is described by a piecewise function, with different power-law dependencies on frequency for low and high frequencies [113]

$$\Omega_{\text{GW}} h^2 = \begin{cases} \Omega_{\text{GW}}(t_0)_p h^2 \left(\frac{f}{f_{p,0}} \right)^3, & f \leq f_{p,0} \\ \Omega_{\text{GW}}(t_0)_p h^2 \left(\frac{f_{p,0}}{f} \right), & f > f_{p,0} \end{cases} \quad (5.15)$$

where h represents the reduced Hubble parameter, $f_{p,0}$ and $\Omega_{\text{GW}}(t_0)_p$ represent the present peak frequency and amplitude, respectively.

In a two-axion mixing scenario [69], we predict the gravitational waves spectra with the peak frequency of approximately 0.2 nHz and the peak amplitude of around 5×10^{-9} , which can be tested by future pulsar timing array (PTA) projects.

5.6 Primordial black holes

Similarly, primordial black holes can also form from the collapse of these domain walls, and even result in the formation of supermassive black holes [69–71]. The closed domain

walls can shrink to the Schwarzschild radius during their annihilation and subsequently collapse into primordial black holes [114, 115]. The collapse of these domain walls is considered to occur in an approximately spherically symmetric manner [116, 117]. Specifically, the fraction of primordial black holes can be described by [69]

$$f_{\text{PBH}} \simeq 4 \left(\frac{45 m_{\text{Pl}}^6}{64 \pi^3} \right)^{(\alpha+1)/4} \frac{g_{*s}(T_0)}{g_*(T_0)} \frac{g_*(T_f)^{(3-\alpha)/4}}{g_{*s}(T_f)} \frac{M_{\text{PBH}}^{-(\alpha+1)/2}}{T_{\text{ann}}^\alpha T_0} \frac{\rho_R(T_0)}{\rho_{\text{DM}}(T_0)}, \quad (5.16)$$

where m_{Pl} is the Planck mass, α is a positive parameter [118], T_{ann} is the domain walls annihilation temperature, T_f is the primordial black holes formation temperature, M_{PBH} is the primordial black holes mass, ρ_R and ρ_{DM} are the radiation and dark matter energy densities, respectively.

We also demonstrate that primordial black holes, within a mass range of $\mathcal{O}(10^5 - 10^8) M_\odot$, could potentially form in a two-axion mixing scenario, accounting for approximately 10^{-5} of the cold dark matter [69]. Furthermore, the two-axion mixing has an impact on another formation mechanism of primordial black holes [74, 119], as well as on the formation of supermassive black holes at high redshifts [120].

6 Conclusion and outlook

In summary, we have investigated axion mass mixing within the framework of type IIB string theory, focusing on the LVS axiverse. Our exploration began with an overview of axions in string theory, with model-independent and model-dependent axions. We then transitioned to a review of the type IIB string axiverse, emphasizing the significance of the LVS in realizing an axiverse potential. Within this context, we have presented several specific LVS axiverse models, such as the one featuring one QCD axion plus one ALP, one QCD axion plus two ALPs, and even more complex scenarios involving one QCD axion plus multiple ALPs. These models naturally correspond to the mixing scenarios of $1 + 1$, $1 + 2$, and $1 + N$ ($N > 2$), where the 1 denotes the number of the QCD axion and the N signifies the number of ALPs, with each scenario featuring unique axion masses and decay constants. Notice that the mixing scenarios presented here, involving more than two axions, have never been studied before.

Our investigation of axion mass mixing revealed crucial insights. Through detailed analysis, we have derived the mass mixing matrices and their corresponding eigenvalues, which have enabled us to understand the complex dynamics of axion mass eigenstates in the mixing. Notably, we found that maximal mixing among multiple axion mass eigenstates occurs under specific conditions: the masses of all ALPs must be smaller than the mass of the QCD axion, with no two ALP masses being equal; and the decay constants of all ALPs must uniformly be either smaller or larger than the decay constant

of the QCD axion. We also found that the transfer of axion energy density ultimately only occurs between the two axions with the closest masses. These insights set the stage for understanding axion dynamics within the type IIB string axiverse, and can also be applicable to more generalized multi-axion mixing scenarios.

Moreover, we delved into the cosmological implications of axion mass mixing, including its potential roles in dark matter, isocurvature fluctuations, dark energy, domain walls, gravitational waves, and primordial black holes. The rich phenomenology, particularly within the context of the LVS axiverse, offers intriguing possibilities for addressing some of the most pressing questions in modern cosmology.

The string axiverse presents a fascinating and complex landscape for axion physics. Our study has provided a detailed examination of its various facets, from axion models and mass mixing to cosmological implications. As we continue to unravel the mysteries of the Universe, the axiverse remains a promising arena for theoretical and observational exploration. Future work in this area will undoubtedly deepen our understanding of axions and their potential roles within the broader context of axion physics.

Acknowledgments

We thank Michele Cicoli for useful discussions. This work was supported by the CAS Project for Young Scientists in Basic Research YSBR-006, the National Key R&D Program of China (Grant No. 2017YFA0402204), and the National Natural Science Foundation of China (NSFC) (Grants No. 11821505, No. 11825506, and No. 12047503).

A Divisor volumes

Consider the orientifold projections $h_-^{1,1} = 0 \rightarrow h_+^{1,1} = h_+^{1,1}$, and define $\{\hat{D}_i\}_{i=1}^{h_+^{1,1}}$ as a basis of $H^{1,1}(X, \mathbb{Z})$, the Kähler form can be described by

$$J = t^i \hat{D}_i, \tag{A.1}$$

where t^i represent the sets of real coordinates on the space of J , and each two-form \hat{D}_i is Poincaré dual to the divisor D_i . The volume of the internal manifold is given by

$$\mathcal{V} = \frac{1}{3!} \int_X J \wedge J \wedge J = \frac{1}{3!} k_{ijk} t^i t^j t^k, \tag{A.2}$$

where k_{ijk} are the triple intersection numbers

$$k_{ijk} = \int_X \hat{D}_i \wedge \hat{D}_j \wedge \hat{D}_k = D_i \cdot D_j \cdot D_k. \tag{A.3}$$

The natural holomorphic coordinates which appear in type IIB flux compactifications are the Einstein-frame volumes of the divisor

$$\tau_i = \frac{1}{2} \int_X \hat{D}_i \wedge J \wedge J = \frac{\partial \mathcal{V}}{\partial t^i} = \frac{1}{2} k_{ijk} t^j t^k. \quad (\text{A.4})$$

This transformation of coordinates amounts to a Legendre transform on \mathcal{V} . The Kähler potential is determined as

$$\mathcal{K} = \frac{K}{M_{\text{Pl}}^2} = -2 \ln \mathcal{V}, \quad \mathcal{K}_{ij} = \frac{\partial \mathcal{K}}{\partial \tau_i \partial \tau_j}, \quad \mathcal{K}^{ij} = \tau_i \tau_j - k_{ijk} t^k \mathcal{V}. \quad (\text{A.5})$$

B Axion coupling to gauge fields

The axion coupling to gauge field strengths originates from the KK reduction of the Chern-Simons (CS) term within the action of D-branes. Considering the axion fields c^a and c_α , the effective Lagrangian is given by [37]

$$\begin{aligned} \mathcal{L} \supset & -\frac{e^\Phi}{4\mathcal{V}^2} \left(dc^a + \frac{M_{\text{Pl}}}{2\pi} e^{-\Phi} \mathcal{A}_i r^{ia} \right) \mathcal{K}^{ab} \wedge \star \left(dc^b + \frac{M_{\text{Pl}}}{2\pi} e^{-\Phi} \mathcal{A}_j r^{jb} \right) \\ & - \frac{1}{8} \left(dc_\alpha + \frac{M_{\text{Pl}}}{\pi} \mathcal{A}_i q_{i\alpha} \right) \mathcal{K}^{\alpha\beta} \wedge \star \left(dc_\beta + \frac{M_{\text{Pl}}}{\pi} \mathcal{A}_j q_{j\beta} \right) \\ & + \frac{M_{\text{Pl}}^2}{4\pi^2 \mathcal{V}^2} e^{-\Phi} \mathcal{A}_i \mathcal{A}_j r^{ia} r^{jb} \mathcal{K}^{ab} + \frac{M_{\text{Pl}}^2}{8\pi^2} \mathcal{A}_i \mathcal{A}_j q_{i\alpha} q_{j\beta} \mathcal{K}_{\alpha\beta} \\ & + \frac{1}{4\pi M_{\text{Pl}}} \left(q_{ia} c^a + r^{i\alpha} c_\alpha \right) \text{Tr}(F \wedge F) - \frac{r^{i\alpha} \tau_\alpha}{4\pi M_{\text{Pl}}} \text{Tr}(F_i \wedge \star F_i), \end{aligned} \quad (\text{B.1})$$

where Φ represents the axio-dilaton, \mathcal{A}_i are the U(1) gauge bosons, r^{ia} and $q_{i\alpha}$ are the couplings of the two-forms. Notice that the orientifold-odd fields c^a have decay constants that are equal to or larger than the string scale, rendering them negligible. Therefore, we focus on the case where $h_-^{1,1} = 0$.

C Axion relic density without mass mixing

Here we show the axion relic density without mass mixing via the misalignment mechanism. Notice that we just consider the pre-inflationary scenario where the PQ symmetry is spontaneously broken during inflation. The temperature-dependent QCD axion mass can be described by

$$m_{a_0}(T) = \begin{cases} m_{a_0,0}, & T \leq T_{\text{QCD}} \\ m_{a_0,0} \left(\frac{T}{T_{\text{QCD}}} \right)^{-b}, & T > T_{\text{QCD}} \end{cases}, \quad (\text{C.1})$$

where $T_{\text{QCD}} \simeq 150 \text{ MeV}$ is the QCD phase transition critical temperature, and $b \simeq 4.08$ is an index taken from the dilute instanton gas approximation [121]. The zero-temperature QCD axion mass is given by [122]

$$m_{a_0,0} = \frac{m_\pi f_\pi}{f_{a_0}} \frac{\sqrt{m_u m_d}}{m_u + m_d}, \quad (\text{C.2})$$

where m_π and f_π are the mass and decay constant of the pion, respectively, m_u and m_d are the up and down quark masses.

At high cosmic temperatures $T \gg T_{\text{QCD}}$, the QCD axion field remains frozen at its initial misalignment angle θ_i . As the temperature decreases, it begins to oscillate when its mass becomes comparable to the Hubble parameter. The oscillation temperature T_{osc,a_0} is given by

$$m_{a_0}(T_{\text{osc},a_0}) = 3H(T_{\text{osc},a_0}), \quad (\text{C.3})$$

with the Hubble parameter

$$H(T) = \sqrt{\frac{\pi^2 g_*(T)}{90}} \frac{T^2}{M_{\text{Pl}}}. \quad (\text{C.4})$$

The axion initial energy density at T_{osc,a_0} is

$$\rho_{a_0,\text{osc}} = \frac{1}{2} m_{a_0,\text{osc}}^2 f_{a_0}^2 \theta_i^2, \quad (\text{C.5})$$

where $m_{a_0,\text{osc}}$ is the axion mass at T_{osc,a_0} . For temperatures $T_0 < T < T_{1,a}$, the QCD axion energy density is adiabatic invariant with the comoving number

$$N_{a_0} \equiv \frac{\rho_{a_0}}{m_{a_0}} \mathbf{a}^3, \quad (\text{C.6})$$

where \mathbf{a} is the scale factor. Using

$$\frac{\rho_{a_0,\text{osc}} \mathbf{a}_{\text{osc},a_0}^3}{m_{a_0,\text{osc}}} = \frac{\rho_{a_0,0} \mathbf{a}_0^3}{m_{a_0,0}}, \quad (\text{C.7})$$

we can derive the QCD axion energy density at present

$$\rho_{a_0,0} = \frac{1}{2} m_{a_0,0} m_{a_0,\text{osc}} f_{a_0}^2 \theta_i^2 \left(\frac{\mathbf{a}_{\text{osc},a_0}}{\mathbf{a}_0} \right)^3, \quad (\text{C.8})$$

where $\mathbf{a}_{\text{osc},a_0}$ and \mathbf{a}_0 are the scale factors at T_{osc,a_0} and T_0 , respectively. More precisely, the current QCD axion dark matter abundance is given by [62]

$$\Omega_{a_0} h^2 \simeq 0.14 \left(\frac{g_{*s}(T_0)}{3.94} \right) \left(\frac{g_*(T_{\text{osc},a_0})}{61.75} \right)^{-0.42} \left(\frac{f_{a_0}}{10^{12} \text{ GeV}} \right)^{1.16} \langle \theta_i^2 f(\theta_i) \rangle, \quad (\text{C.9})$$

where $f(\theta_i)$ is the anharmonicity factor [123, 124]. In order to explain the observed dark matter abundance, we require an $\sim \mathcal{O}(1)$ initial misalignment angle

$$\theta_i \simeq 0.87 \left(\frac{g_{*s}(T_0)}{3.94} \right)^{-1/2} \left(\frac{g_*(T_{\text{osc},a_0})}{61.75} \right)^{0.21} \left(\frac{f_{a_0}}{10^{12} \text{ GeV}} \right)^{-0.58}. \quad (\text{C.10})$$

Similarly, for the single-field ALP dark matter with a constant mass m_{A_i} , its abundance can be expressed as [62]

$$\begin{aligned} \Omega_{A_i} h^2 \simeq & 0.95 \left(\frac{g_{*s}(T_0)}{3.94} \right) \left(\frac{g_*(T_{\text{osc},A_i})}{61.75} \right)^{-1} \\ & \times \left(\frac{m_{A_i}}{1 \text{ eV}} \right)^{1/2} \left(\frac{f_{A_i}}{10^{12} \text{ GeV}} \right)^2 \langle \Theta_{i,A_i}^2 f(\Theta_{i,A_i}) \rangle. \end{aligned} \quad (\text{C.11})$$

References

- [1] A. Arvanitaki, S. Dimopoulos, S. Dubovsky, N. Kaloper and J. March-Russell, *String Axiverse*, *Phys. Rev. D* **81** (2010) 123530, [0905.4720].
- [2] M. Demirtas, C. Long, L. McAllister and M. Stillman, *The Kreuzer-Skarke Axiverse*, *JHEP* **04** (2020) 138, [1808.01282].
- [3] M. Reig, *The stochastic axiverse*, *JHEP* **09** (2021) 207, [2104.09923].
- [4] M. Demirtas, N. Gendler, C. Long, L. McAllister and J. Moritz, *PQ axiverse*, *JHEP* **06** (2023) 092, [2112.04503].
- [5] R. Peccei and H. R. Quinn, *CP Conservation in the Presence of Instantons*, *Phys. Rev. Lett.* **38** (1977) 1440–1443.
- [6] R. Peccei and H. R. Quinn, *Constraints Imposed by CP Conservation in the Presence of Instantons*, *Phys. Rev. D* **16** (1977) 1791–1797.
- [7] S. Weinberg, *A New Light Boson?*, *Phys. Rev. Lett.* **40** (1978) 223–226.
- [8] F. Wilczek, *Problem of Strong P and T Invariance in the Presence of Instantons*, *Phys. Rev. Lett.* **40** (1978) 279–282.
- [9] J. E. Kim, *Weak Interaction Singlet and Strong CP Invariance*, *Phys. Rev. Lett.* **43** (1979) 103.
- [10] M. A. Shifman, A. I. Vainshtein and V. I. Zakharov, *Can Confinement Ensure Natural CP Invariance of Strong Interactions?*, *Nucl. Phys. B* **166** (1980) 493–506.
- [11] M. Dine, W. Fischler and M. Srednicki, *A Simple Solution to the Strong CP Problem with a Harmless Axion*, *Phys. Lett. B* **104** (1981) 199–202.
- [12] A. R. Zhitnitsky, *On Possible Suppression of the Axion Hadron Interactions. (In Russian)*, *Sov. J. Nucl. Phys.* **31** (1980) 260.

- [13] G. 't Hooft, *Symmetry Breaking Through Bell-Jackiw Anomalies*, *Phys. Rev. Lett.* **37** (1976) 8–11.
- [14] G. 't Hooft, *Computation of the Quantum Effects Due to a Four-Dimensional Pseudoparticle*, *Phys. Rev. D* **14** (1976) 3432–3450.
- [15] J. Preskill, M. B. Wise and F. Wilczek, *Cosmology of the Invisible Axion*, *Phys. Lett. B* **120** (1983) 127–132.
- [16] L. Abbott and P. Sikivie, *A Cosmological Bound on the Invisible Axion*, *Phys. Lett. B* **120** (1983) 133–136.
- [17] M. Dine and W. Fischler, *The Not So Harmless Axion*, *Phys. Lett. B* **120** (1983) 137–141.
- [18] D. J. E. Marsh, *Axion Cosmology*, *Phys. Rept.* **643** (2016) 1–79, [[1510.07633](#)].
- [19] L. Di Luzio, M. Giannotti, E. Nardi and L. Visinelli, *The landscape of QCD axion models*, *Phys. Rept.* **870** (2020) 1–117, [[2003.01100](#)].
- [20] C. A. J. O'Hare, *Cosmology of axion dark matter*, *PoS COSMICWISPerS* (2024) 040, [[2403.17697](#)].
- [21] A. Hook, *TASI Lectures on the Strong CP Problem and Axions*, *PoS TASI2018* (2019) 004, [[1812.02669](#)].
- [22] G. Raffelt and D. Seckel, *Bounds on Exotic Particle Interactions from SN 1987a*, *Phys. Rev. Lett.* **60** (1988) 1793.
- [23] M. S. Turner, *Axions from SN 1987a*, *Phys. Rev. Lett.* **60** (1988) 1797.
- [24] R. Mayle, J. R. Wilson, J. R. Ellis, K. A. Olive, D. N. Schramm and G. Steigman, *Constraints on Axions from SN 1987a*, *Phys. Lett. B* **203** (1988) 188–196.
- [25] L. B. Leinson, *Axion mass limit from observations of the neutron star in Cassiopeia A*, *JCAP* **08** (2014) 031, [[1405.6873](#)].
- [26] K. Hamaguchi, N. Nagata, K. Yanagi and J. Zheng, *Limit on the Axion Decay Constant from the Cooling Neutron Star in Cassiopeia A*, *Phys. Rev. D* **98** (2018) 103015, [[1806.07151](#)].
- [27] M. Buschmann, C. Dessert, J. W. Foster, A. J. Long and B. R. Safdi, *Upper Limit on the QCD Axion Mass from Isolated Neutron Star Cooling*, *Phys. Rev. Lett.* **128** (2022) 091102, [[2111.09892](#)].
- [28] E. Witten, *Some Properties of $O(32)$ Superstrings*, *Phys. Lett. B* **149** (1984) 351–356.
- [29] M. B. Green and J. H. Schwarz, *Anomaly Cancellation in Supersymmetric $D=10$ Gauge Theory and Superstring Theory*, *Phys. Lett. B* **149** (1984) 117–122.
- [30] K.-w. Choi, *A QCD axion from higher dimensional gauge field*, *Phys. Rev. Lett.* **92** (2004) 101602, [[hep-ph/0308024](#)].

- [31] P. Svrcek and E. Witten, *Axions In String Theory*, *JHEP* **06** (2006) 051, [[hep-th/0605206](#)].
- [32] J. P. Conlon, *The QCD axion and moduli stabilisation*, *JHEP* **05** (2006) 078, [[hep-th/0602233](#)].
- [33] N. Gendler and C. Vafa, *Axions in the dark dimension*, *JHEP* **12** (2024) 127, [[2404.15414](#)].
- [34] M. Reece, *Extra-Dimensional Axion Expectations*, [2406.08543](#).
- [35] K. Choi and N. Righi, *Axion theory and model building*, *PoS COSMICWISPers* (2024) 039, [[2401.17354](#)].
- [36] B. S. Acharya, K. Bobkov and P. Kumar, *An M Theory Solution to the Strong CP Problem and Constraints on the Axiverse*, *JHEP* **11** (2010) 105, [[1004.5138](#)].
- [37] M. Cicoli, M. Goodsell and A. Ringwald, *The type IIB string axiverse and its low-energy phenomenology*, *JHEP* **10** (2012) 146, [[1206.0819](#)].
- [38] M. Cicoli, C. Mayrhofer and R. Valandro, *Moduli Stabilisation for Chiral Global Models*, *JHEP* **02** (2012) 062, [[1110.3333](#)].
- [39] M. Cicoli, G. Tasinato, I. Zavala, C. P. Burgess and F. Quevedo, *Modulated Reheating and Large Non-Gaussianity in String Cosmology*, *JCAP* **05** (2012) 039, [[1202.4580](#)].
- [40] I. Broeckel, M. Cicoli, A. Maharana, K. Singh and K. Sinha, *Moduli stabilisation and the statistics of axion physics in the landscape*, *JHEP* **08** (2021) 059, [[2105.02889](#)]. [Addendum: *JHEP* 01, 191 (2022)].
- [41] G. D. Coughlan, W. Fischler, E. W. Kolb, S. Raby and G. G. Ross, *Cosmological Problems for the Polonyi Potential*, *Phys. Lett. B* **131** (1983) 59–64.
- [42] B. de Carlos, J. A. Casas, F. Quevedo and E. Roulet, *Model independent properties and cosmological implications of the dilaton and moduli sectors of 4-d strings*, *Phys. Lett. B* **318** (1993) 447–456, [[hep-ph/9308325](#)].
- [43] T. Banks, D. B. Kaplan and A. E. Nelson, *Cosmological implications of dynamical supersymmetry breaking*, *Phys. Rev. D* **49** (1994) 779–787, [[hep-ph/9308292](#)].
- [44] S. Kachru, R. Kallosh, A. D. Linde and S. P. Trivedi, *De Sitter vacua in string theory*, *Phys. Rev. D* **68** (2003) 046005, [[hep-th/0301240](#)].
- [45] V. Balasubramanian, P. Berglund, J. P. Conlon and F. Quevedo, *Systematics of moduli stabilisation in Calabi-Yau flux compactifications*, *JHEP* **03** (2005) 007, [[hep-th/0502058](#)].
- [46] R. Blumenhagen, J. P. Conlon, S. Krippendorff, S. Moster and F. Quevedo, *SUSY Breaking in Local String/F-Theory Models*, *JHEP* **09** (2009) 007, [[0906.3297](#)].

- [47] M. Cicoli, J. P. Conlon and F. Quevedo, *General Analysis of LARGE Volume Scenarios with String Loop Moduli Stabilisation*, *JHEP* **10** (2008) 105, [[0805.1029](#)].
- [48] C. T. Hill and G. G. Ross, *Models and New Phenomenological Implications of a Class of Pseudogoldstone Bosons*, *Nucl. Phys. B* **311** (1988) 253–297.
- [49] R. Daido, N. Kitajima and F. Takahashi, *Level crossing between the QCD axion and an axionlike particle*, *Phys. Rev. D* **93** (2016) 075027, [[1510.06675](#)].
- [50] D. Cyncynates and J. O. Thompson, *Heavy QCD axion dark matter from avoided level crossing*, *Phys. Rev. D* **108** (2023) L091703, [[2306.04678](#)].
- [51] H.-J. Li, Y.-Q. Peng, W. Chao and Y.-F. Zhou, *Light QCD axion dark matter from double level crossings*, *Phys. Lett. B* **849** (2024) 138444, [[2310.02126](#)].
- [52] A. Hook, *Solving the Hierarchy Problem Discretely*, *Phys. Rev. Lett.* **120** (2018) 261802, [[1802.10093](#)].
- [53] L. Di Luzio, B. Gavela, P. Quilez and A. Ringwald, *An even lighter QCD axion*, *JHEP* **05** (2021) 184, [[2102.00012](#)].
- [54] L. Di Luzio, B. Gavela, P. Quilez and A. Ringwald, *Dark matter from an even lighter QCD axion: trapped misalignment*, *JCAP* **10** (2021) 001, [[2102.01082](#)].
- [55] H.-J. Li, *On the temperature effects in QCD axion mass mixing*, [2410.00377](#).
- [56] L. Wolfenstein, *Neutrino Oscillations in Matter*, *Phys. Rev. D* **17** (1978) 2369–2374.
- [57] S. P. Mikheyev and A. Y. Smirnov, *Resonance Amplification of Oscillations in Matter and Spectroscopy of Solar Neutrinos*, *Sov. J. Nucl. Phys.* **42** (1985) 913–917.
- [58] S. P. Mikheev and A. Y. Smirnov, *Resonant amplification of neutrino oscillations in matter and solar neutrino spectroscopy*, *Nuovo Cim. C* **9** (1986) 17–26.
- [59] S.-Y. Ho, K. Saikawa and F. Takahashi, *Enhanced photon coupling of ALP dark matter adiabatically converted from the QCD axion*, *JCAP* **10** (2018) 042, [[1806.09551](#)].
- [60] D. Cyncynates, T. Giurgica-Tiron, O. Simon and J. O. Thompson, *Resonant nonlinear pairs in the axiverse and their late-time direct and astrophysical signatures*, *Phys. Rev. D* **105** (2022) 055005, [[2109.09755](#)].
- [61] K. Murai, F. Takahashi and W. Yin, *QCD axion: A unique player in the axiverse with mixings*, *Phys. Rev. D* **108** (2023) 036020, [[2305.18677](#)].
- [62] H.-J. Li, *Axion dark matter with explicit Peccei-Quinn symmetry breaking in the axiverse*, *JCAP* **09** (2024) 025, [[2307.09245](#)].
- [63] K. Murai, Y. Narita, F. Takahashi and W. Yin, *QCD Axion Dark Matter from level crossing with refined adiabatic condition*, [2412.10232](#).
- [64] N. Kitajima and F. Takahashi, *Resonant conversions of QCD axions into hidden axions and suppressed isocurvature perturbations*, *JCAP* **01** (2015) 032, [[1411.2011](#)].

- [65] K. Müürsepp, E. Nardi and C. Smarra, *Can the QCD axion feed a dark energy component?*, [2405.00090](#).
- [66] K. Müürsepp, *On the viability of the QCD axion - dark energy transition*, 5, 2024. [2405.20478](#).
- [67] R. Daido, N. Kitajima and F. Takahashi, *Domain Wall Formation from Level Crossing in the Axiverse*, *Phys. Rev. D* **92** (2015) 063512, [[1505.07670](#)].
- [68] J. Lee, K. Murai, F. Takahashi and W. Yin, *More is Different: Multi-Axion Dynamics Changes Topological Defect Evolution*, [2409.09749](#).
- [69] H.-J. Li and Y.-F. Zhou, *Gravitational waves and primordial black holes from axion domain walls in level crossing**, *Chin. Phys. C* **49** (2025) 035101, [[2401.09138](#)].
- [70] D. Cyncynates, O. Simon, J. O. Thompson and Z. J. Weiner, *Nonperturbative structure in coupled axion sectors and implications for direct detection*, *Phys. Rev. D* **106** (2022) 083503, [[2208.05501](#)].
- [71] Z. Chen, A. Kobakhidze, C. A. J. O'Hare, Z. S. C. Picker and G. Pierobon, *Cosmology of the companion-axion model: dark matter, gravitational waves, and primordial black holes*, [2110.11014](#).
- [72] N. Kitajima, J. Lee, K. Murai, F. Takahashi and W. Yin, *Gravitational waves from domain wall collapse, and application to nanohertz signals with QCD-coupled axions*, *Phys. Lett. B* **851** (2024) 138586, [[2306.17146](#)].
- [73] J. Lee, K. Murai, F. Takahashi and W. Yin, *Induced domain walls of QCD axion, and gravitational waves*, *JCAP* **10** (2024) 038, [[2407.09478](#)].
- [74] H.-J. Li, *QCD axion bubbles in the presence of ALP resonant conversion*, *Commun. Theor. Phys.* **xx** (2025) xx, [[2303.04537](#)].
- [75] H.-J. Li and Y.-F. Zhou, *Mass mixing between QCD axions*, [2408.00267](#).
- [76] A. Arvanitaki and S. Dubovsky, *Exploring the String Axiverse with Precision Black Hole Physics*, *Phys. Rev. D* **83** (2011) 044026, [[1004.3558](#)].
- [77] D. J. E. Marsh, *The Axiverse Extended: Vacuum Destabilisation, Early Dark Energy and Cosmological Collapse*, *Phys. Rev. D* **83** (2011) 123526, [[1102.4851](#)].
- [78] D. J. E. Marsh, D. Grin, R. Hlozek and P. G. Ferreira, *Axiverse cosmology and the energy scale of inflation*, *Phys. Rev. D* **87** (2013) 121701, [[1303.3008](#)].
- [79] H. Tashiro, J. Silk and D. J. E. Marsh, *Constraints on primordial magnetic fields from CMB distortions in the axiverse*, *Phys. Rev. D* **88** (2013) 125024, [[1308.0314](#)].
- [80] H. Yoshino and H. Kodama, *Probing the string axiverse by gravitational waves from Cygnus X-1*, *PTEP* **2015** (2015) 061E01, [[1407.2030](#)].

- [81] M. Kamionkowski, J. Pradler and D. G. E. Walker, *Dark energy from the string axiverse*, *Phys. Rev. Lett.* **113** (2014) 251302, [[1409.0549](#)].
- [82] H. Yoshino and H. Kodama, *The bosenova and axiverse*, *Class. Quant. Grav.* **32** (2015) 214001, [[1505.00714](#)].
- [83] B. S. Acharya and C. Pongkitivanichkul, *The Axiverse induced Dark Radiation Problem*, *JHEP* **04** (2016) 009, [[1512.07907](#)].
- [84] R. Emami, D. Grin, J. Pradler, A. Raccanelli and M. Kamionkowski, *Cosmological tests of an axiverse-inspired quintessence field*, *Phys. Rev. D* **93** (2016) 123005, [[1603.04851](#)].
- [85] T. Karwal and M. Kamionkowski, *Dark energy at early times, the Hubble parameter, and the string axiverse*, *Phys. Rev. D* **94** (2016) 103523, [[1608.01309](#)].
- [86] E. Hardy, *Miniclusters in the Axiverse*, *JHEP* **02** (2017) 046, [[1609.00208](#)].
- [87] D. Yoshida and J. Soda, *Exploring the string axiverse and parity violation in gravity with gravitational waves*, *Int. J. Mod. Phys. D* **27** (2018) 1850096, [[1708.09592](#)].
- [88] N. Kitajima, J. Soda and Y. Urakawa, *Gravitational wave forest from string axiverse*, *JCAP* **10** (2018) 008, [[1807.07037](#)].
- [89] P. Agrawal, A. Hook and J. Huang, *A CMB Millikan experiment with cosmic axiverse strings*, *JHEP* **07** (2020) 138, [[1912.02823](#)].
- [90] M. Calzà, J. March-Russell and J. a. G. Rosa, *Evaporating Primordial Black Holes, the String Axiverse, and Hot Dark Radiation*, *Phys. Rev. Lett.* **133** (2024) 261003, [[2110.13602](#)].
- [91] M. Calzà, J. a. G. Rosa and F. Serrano, *Primordial black hole superradiance and evaporation in the string axiverse*, *JHEP* **05** (2024) 140, [[2306.09430](#)].
- [92] S. Alexander, H. Gilmer, T. Manton and E. McDonough, *π -axion and π -axiverse of dark QCD*, *Phys. Rev. D* **108** (2023) 123014, [[2304.11176](#)].
- [93] S. Gasparotto and E. I. Sfakianakis, *Cosmic birefringence from the Axiverse*, *JCAP* **11** (2023) 017, [[2306.16355](#)].
- [94] N. Gendler, D. J. E. Marsh, L. McAllister and J. Moritz, *Glimmers from the axiverse*, *JCAP* **09** (2024) 071, [[2309.13145](#)].
- [95] L. Martucci, N. Risso, A. Valenti and L. Vecchi, *Wormholes in the axiverse, and the species scale*, *JHEP* **07** (2024) 240, [[2404.14489](#)].
- [96] S. Das and F. Ferrer, *Gravitational waves from the Axiverse*, [2502.12153](#).
- [97] M.-S. Seo, *Axion species scale and axion weak gravity conjecture-like bound*, *JHEP* **11** (2024) 082, [[2407.16156](#)].

- [98] F. Denef, M. R. Douglas and B. Florea, *Building a better racetrack*, *JHEP* **06** (2004) 034, [[hep-th/0404257](#)].
- [99] M. Cicoli, M. Kreuzer and C. Mayrhofer, *Toric K3-Fibred Calabi-Yau Manifolds with del Pezzo Divisors for String Compactifications*, *JHEP* **02** (2012) 002, [[1107.0383](#)].
- [100] J. P. Conlon, F. Quevedo and K. Suruliz, *Large-volume flux compactifications: Moduli spectrum and D3/D7 soft supersymmetry breaking*, *JHEP* **08** (2005) 007, [[hep-th/0505076](#)].
- [101] K. Becker, M. Becker, M. Haack and J. Louis, *Supersymmetry breaking and alpha-prime corrections to flux induced potentials*, *JHEP* **06** (2002) 060, [[hep-th/0204254](#)].
- [102] M. Cicoli, J. P. Conlon and F. Quevedo, *Systematics of String Loop Corrections in Type IIB Calabi-Yau Flux Compactifications*, *JHEP* **01** (2008) 052, [[0708.1873](#)].
- [103] M. Cicoli, S. Krippendorf, C. Mayrhofer, F. Quevedo and R. Valandro, *D-Branes at del Pezzo Singularities: Global Embedding and Moduli Stabilisation*, *JHEP* **09** (2012) 019, [[1206.5237](#)].
- [104] M. Cicoli, S. Krippendorf, C. Mayrhofer, F. Quevedo and R. Valandro, *D3/D7 Branes at Singularities: Constraints from Global Embedding and Moduli Stabilisation*, *JHEP* **07** (2013) 150, [[1304.0022](#)].
- [105] M. Cicoli, D. Klevers, S. Krippendorf, C. Mayrhofer, F. Quevedo and R. Valandro, *Explicit de Sitter Flux Vacua for Global String Models with Chiral Matter*, *JHEP* **05** (2014) 001, [[1312.0014](#)].
- [106] H.-J. Li, *QCD axion dark matter in the dark dimension*, [2412.19426](#).
- [107] PLANCK collaboration, N. Aghanim et al., *Planck 2018 results. VI. Cosmological parameters*, *Astron. Astrophys.* **641** (2020) A6, [[1807.06209](#)]. [Erratum: *Astron.Astrophys.* 652, C4 (2021)].
- [108] PLANCK collaboration, Y. Akrami et al., *Planck 2018 results. X. Constraints on inflation*, *Astron. Astrophys.* **641** (2020) A10, [[1807.06211](#)].
- [109] W. H. Press, B. S. Ryden and D. N. Spergel, *Dynamical Evolution of Domain Walls in an Expanding Universe*, *Astrophys. J.* **347** (1989) 590–604.
- [110] M. Hindmarsh, *Analytic scaling solutions for cosmic domain walls*, *Phys. Rev. Lett.* **77** (1996) 4495–4498, [[hep-ph/9605332](#)].
- [111] T. Garagounis and M. Hindmarsh, *Scaling in numerical simulations of domain walls*, *Phys. Rev. D* **68** (2003) 103506, [[hep-ph/0212359](#)].
- [112] J. C. R. E. Oliveira, C. J. A. P. Martins and P. P. Avelino, *The Cosmological evolution of domain wall networks*, *Phys. Rev. D* **71** (2005) 083509, [[hep-ph/0410356](#)].

- [113] T. Hiramatsu, M. Kawasaki and K. Saikawa, *On the estimation of gravitational wave spectrum from cosmic domain walls*, *JCAP* **02** (2014) 031, [[1309.5001](#)].
- [114] F. Ferrer, E. Masso, G. Panico, O. Pujolas and F. Rompineve, *Primordial Black Holes from the QCD axion*, *Phys. Rev. Lett.* **122** (2019) 101301, [[1807.01707](#)].
- [115] S. Ge, J. Guo and J. Liu, *New mechanism for primordial black hole formation from the QCD axion*, *Phys. Rev. D* **109** (2024) 123030, [[2309.01739](#)].
- [116] G. B. Gelmini, A. Simpson and E. Vitagliano, *Catastrogenesis: DM, GWs, and PBHs from ALP string-wall networks*, *JCAP* **02** (2023) 031, [[2207.07126](#)].
- [117] G. B. Gelmini, J. Hyman, A. Simpson and E. Vitagliano, *Primordial black hole dark matter from catastrogenesis with unstable pseudo-Goldstone bosons*, *JCAP* **06** (2023) 055, [[2303.14107](#)].
- [118] M. Kawasaki, K. Saikawa and T. Sekiguchi, *Axion dark matter from topological defects*, *Phys. Rev. D* **91** (2015) 065014, [[1412.0789](#)].
- [119] N. Kitajima and F. Takahashi, *Primordial Black Holes from QCD Axion Bubbles*, *JCAP* **11** (2020) 060, [[2006.13137](#)].
- [120] H.-J. Li, Y.-Q. Peng, W. Chao and Y.-F. Zhou, *Supermassive black holes triggered by QCD axion bubbles*, *Commun. Theor. Phys.* **76** (2024) 055405, [[2304.00939](#)].
- [121] S. Borsanyi et al., *Calculation of the axion mass based on high-temperature lattice quantum chromodynamics*, *Nature* **539** (2016) 69–71, [[1606.07494](#)].
- [122] G. Grilli di Cortona, E. Hardy, J. Pardo Vega and G. Villadoro, *The QCD axion, precisely*, *JHEP* **01** (2016) 034, [[1511.02867](#)].
- [123] D. H. Lyth, *Axions and inflation: Sitting in the vacuum*, *Phys. Rev. D* **45** (1992) 3394–3404.
- [124] L. Visinelli and P. Gondolo, *Dark Matter Axions Revisited*, *Phys. Rev. D* **80** (2009) 035024, [[0903.4377](#)].